Quasiperiodic instability and chaos in the bad-cavity laser with modulated inversion: Numerical analysis of a Toda oscillator system

Tetsuo Ogawa
Department of Applied Physics, Faculty of Engineering, University of Tokyo, 7-3-1 Hongo, Bunkyo-ku, Tokyo 113, Japan
(Received 19 October 1987)

The exact equivalence between a bad-cavity laser with modulated inversion and a nonlinear oscillator in a Toda potential driven by an external modulation is presented. The dynamical properties of the laser system are investigated in detail by analyzing a Toda oscillator system. The temporal characteristics of the bad-cavity laser under strong modulation are analyzed extensively by numerically investigating the simpler Toda system as a function of two control parameters: the dc component of the population inversion and the modulation amplitude. The system exhibits two kinds of optical chaos: One is the *quasiperiodic chaos* in the region of the intermediate modulation amplitude and the other is the *intermittent kicked chaos* in the region of strong modulation and large dc component of the pumping. The former is well described by a one-dimensional discrete map with a singular invariant probability measure. There are two types of onset of the chaos: quasiperiodic instability (continuous path to chaos) and catastrophic crisis (discontinuous path). The period-doubling cascade of bifurcation is also observed. The simple discrete model of the Toda system is presented to obtain analytically the one-dimensional map function and to understand the effect of the asymmetric potential curvature on yielding chaos.

I. INTRODUCTION

The instabilities and deterministic chaos in lasers have attracted much attention in the last few years.[1-3] From a fundamental point of view, the laser has become an attractive system to study, in great detail and with precision, phenomena which are typical of complex systems far from thermal equilibrium. The study of the semiclassical laser equations has been revived because of their close relation to chaos. Thus the laser becomes a useful tool in the investigation of general properties such as instabilities and deterministic chaos.

On the other hand, the dynamical characteristics of lasers have also attracted the interest of researchers in engineering and experimental fields. Since ultrahigh-time-resolution spectroscopy using temporal incoherent laser light has been proposed,[4-6] a need arises to control the temporal coherency of laser light. Well-controlled optical chaos in lasers appears to be a good candidate as incoherent light. Thus quality control of the laser light has potential applications in many fields.

In previous papers,[7-9] we presented numerical studies of regular and chaotic behaviors of the *multimode laser* system with modulated inversion and showed that the dynamical properties of the laser field are strongly influenced by the cavity quality in addition to the physical control parameters: the dc component of the population inversion and the modulation amplitude. In the case of bad cavity (low-Q cavity),[8,9] important features were that two kinds of optical chaos were observed in two limiting cases: first, when the dc component of the population inversion is very large, and second, when the modulation is fairly strong but the dc component is small. Chaos in the first case results from the intrinsic Lorenz instability.[10,11] On the other hand, the second one is essentially caused by external modulation.

This paper deals with the characteristics of chaos in the second case, that is, the optical chaos in the bad-cavity laser with strongly modulated inversion.[12-19] This chaos will be shown to be induced by the quasiperiodicity between the several incommensurate frequencies: for example, the external modulation frequency, the induced quasiperiodic frequency, and the natural frequency of the system.

We turn our attention to the single resonant mode as the relevant mode for stimulated emission. Because we carry out the low-dimensional dynamical analysis, effects of the many off-resonant modes are neglected. Therefore our laser model is essentially that of the resonant single-mode laser, which is one of the simplest laser models.

The fundamental equations describing the interaction between the electric field and the material system in the laser cavity are the three coupled Maxwell-Bloch equations for the electric field of laser light, the atomic polarization, and the population difference of the material. In the very-low-Q cavity, we can perform the adiabatic elimination of the electric field. The consequent two-dimensional system describes the dynamics of the material system. Under the modulation of the population inversion, this system is exactly equivalent to the nonlinear oscillator, which is the motion of the particle in a Toda potential[20] with damping and with external modulation. The dynamical characteristics of the bad-cavity laser with modulated inversion can be examined by analyzing this Toda system. The advantages of the investigation of the Toda system instead of the original laser system are as follows.

(i) Nonlinear oscillation theory[21,22] is applicable.

Therefore we can employ several methods to examine the nonlinear system, e.g., the perturbation method, the iteration method, the averaging method, the isocline method, and so on.

(ii) The principle of the harmonic balance[21,22] is valid. This is the method of widest utility for obtaining a periodic solution of nonlinear differential equations.

(iii) The motion of an oscillator in the well-known Toda potential is more physically visible than in the complex system like the laser. The spiking pulse train of laser emission corresponds to the simple sinusoidal-wave motion of a Toda oscillator.

In order to examine the dynamical properties of this nonlinear system of the Toda oscillator under stronger modulation, we perform numerical studies to reveal the chaotic behaviors. The first purpose of this paper is to clarify the temporal characteristics of a Toda system,[23,24] that is, the laser with modulated inversion in the bad cavity in the case of arbitrary modulation amplitude. We want to obtain the phase diagram of this system in terms of the temporal response to the external modulation as a function of two control parameters: the dc component of the modulation and the modulation amplitude. In addition, bifurcation diagrams are also inevitable in discussing the effect of the quasiperiodic instabilities on the onset of quasiperiodic chaos.

The second purpose is to clarify the ergodic properties of chaos observed in this system under strong modulation. Two kinds of chaos are observed and show different time developments. One of them is shown to be well approximated by the one-dimensional map.[25,26] This is a characteristic of chaos in the low-dimensional dynamical system. We also discuss the validity of the representation of chaos by the one-dimensional map. In addition, we present a simple discrete model to understand in more detail the chaos in an asymmetric Toda potential in terms of the one-dimensional discrete dynamical system.

In this paper we employ numerical techniques to study the onset and the characteristics of chaos in a Toda system. The analytical study for the periodic states of this system will be shown in a future paper[27] to understand their nonlinear characteristics and stabilities.

The main conclusions of this paper are summarized as follows.

(a) The laser system with modulated inversion in the bad cavity is exactly equivalent, without the rate-equation approximation, to the *nonlinear oscillator in a Toda potential* with external modulation. A numerical analysis is performed to study the dynamical responses of the Toda oscillator to the external modulation. Bifurcation diagrams as a function of the modulation amplitude are obtained to reveal the routes to chaos via the *quasiperiodic instability* and/or the period-doubling bifurcations. The onsets of chaos are due not only to the quasiperiodic instability from the harmonic and/or the subharmonic oscillations but also to the *catastrophic crises.* We have also obtained the phase diagrams of this system for two control parameters.

(b) Two kinds of chaotic behaviors exist under the strong modulation: One is the *quasiperiodic chaos* observed in the vicinity of the quasiperiodic or the subharmonic regions as the modulation amplitude increases, the other is the *intermittent kicked chaos* showing the intermittent pulsing of laser emission in the region of the stronger modulation and large dc component of the pumping.

(c) Chaos in a Toda system can be characterized in terms of its spectral structures, return maps, and invariant measures of the one-dimensional map functions. They show that the quasiperiodic chaos can be well described by a one-dimensional map such as the logistic map. However, some differences from the characteristics of the simple one-dimensional map are also observed; for example, the incompleteness of the period-doubling sequences and the multipeaked and multivalued structures of the mapping function.

(d) We have derived analytically the one-dimensional mapping (transfer) function from a simplified model of a Toda system under the condition of a large population relaxation rate. This analysis shows that the asymmetry of the potential plays an important role in inducing chaotic behaviors.

This paper is organized as follows. In Sec. II the laser equations for the relevant resonant mode with modulated inversion without the rate-equation approximation are transformed into the nonlinear equations of the oscillator in a Toda potential by using the adiabatic elimination of the field variable. We choose the dc component of the population inversion, the modulation amplitude, and the ratio of the longitudinal relaxation constant to the modulation frequency as control parameters. This ratio works as a damping constant of a Toda system. In the two cases of the ratios 1.0 and 0.1, numerical calculations of this system for arbitrary values of two control parameters are performed extensively in Sec. III. The routes and the characteristics of chaos are investigated there. In Sec. IV the simple discrete model is presented to understand chaotic motion as a one-dimensional map, and we obtain analytically the approximate map function. Our conclusions are given in Sec. V.

II. EQUATION OF MOTION

We study the temporal behavior of a traveling-wave field interacting with a homogeneously broadened medium under sinusoidal modulation of a population inversion in a unidirectional ring cavity. Transverse effects of the laser-beam profile are ignored in this paper. The active medium consists of two-level atoms with transition frequency ω_A between lasing levels, and relaxation constants $\gamma_\perp$ and $\gamma_\parallel$ for the polarization and the population, respectively. These atoms are excited for lasing from the outside. The interaction of active atoms with the cavity field in the resonance case is described by the Maxwell-Bloch equations

$$\left[c\frac{\partial}{\partial z}+\frac{\partial}{\partial t}\right]E(z,t)=-KE+igP\ , \tag{1a}$$

$$\frac{\partial}{\partial t}P(z,t)=-\gamma_\perp P-igED\ , \tag{1b}$$

$$\frac{\partial}{\partial t}D(z,t)=-\gamma_\parallel D+\gamma_\parallel D^{(0)}(t)+2ig(EP^*-E^*P)\ , \tag{1c}$$

where E is the complex field envelope, P the atomic polarization envelope, and D the population difference. Here, K is the effective relaxation constant of the field[9] including transmission losses through the cavity mirrors and g is the coupling constant between the field and the matter. Deviation from the ordinary Maxwell-Bloch equations is such that the source term of the population difference is not constant in time. The population inversion term $D^{(0)}(t)$ is modulated from the outside sinusoidally with modulation frequency ω_m and amplitude ζ around its dc component $D^{(0)}$,

$$D^{(0)}(t)=D^{(0)}+\zeta\cos(\omega_m t) . \tag{2}$$

The modulation frequency ω_m should be chosen to be smaller than both the HWHM (half width at half maximum) of the unsaturated gain width $\gamma_\perp$ or the power-broadened linewidth $(g/2)(\gamma_\perp/\gamma_\parallel)^{1/2}|E|$ and the longitudinal mode spacing $2\pi c/L$ of the cavity with length L, in order that the single-mode model be valid.[28] In the case of the single-mode operation, the longitudinal mode spacing is much larger than the unsaturated or the power-broadened linewidth. Therefore the modulation frequency must satisfy the relation $\omega_m<\gamma_\perp$. In order to investigate the dynamical characteristics of the resonant mode for the stimulated emission, we employ the mean-field approximation to eliminate the spatial derivative $\partial/\partial z$. The effects of off-resonant modes and spontaneous emission are neglected in this paper in order to pursue only the temporal evolution of the relevant resonant mode as a low-dimensional *deterministic system*. This is one of the dynamical and deterministic approaches used to clarify the temporal characteristics of lasers. On the other hand, when a great many off-resonant modes operate independently and simultaneously, we can employ stochastic methods, e.g., the nonlinear Langevin equations or the Fokker-Planck equations. Here we concentrate on the dynamical and deterministic aspects of the modulated laser.

In the case of no modulation ($\zeta=0$), the Maxwell-Bloch equations have their steady-state solutions,

$$|E^S|^2=\frac{\gamma_\perp\gamma_\parallel}{4g^2}\left(\frac{D^{(0)}}{D_{\rm th}}-1\right) , \tag{3a}$$

$$P^S=-i\frac{g}{\gamma_\perp}D_{\rm th}E^S , \tag{3b}$$

$$D^S=D_{\rm th}\equiv\frac{K\gamma_\perp}{g^2} . \tag{3c}$$

The lasing threshold is calculated as $D_{\rm th}$ in this mean-field model.

Three variables $E(t)$, $P(t)$, and $D(t)$ are normalized by their steady-state values (3a)–(3c) as

$$\begin{aligned}\hat{E}(t)&=E(t)/|E^S| ,\\ \hat{P}(t)&=P(t)/|P^S| ,\\ \hat{D}(t)&=D(t)/D^S .\end{aligned} \tag{4}$$

These normalized variables obey the following Maxwell-Bloch equations:

$$\begin{aligned}\frac{d}{dt}\hat{E}(t)&=-K\hat{E}+K\hat{P} ,\\ \frac{d}{dt}\hat{P}(t)&=-\gamma_\perp\hat{P}+\gamma_\perp\hat{E}\hat{D} ,\\ \frac{d}{dt}\hat{D}(t)&=-\gamma_\parallel\hat{D}+\gamma_\parallel A+\gamma_\parallel B\cos(\omega_m t)\\ &\quad-\frac{\gamma_\parallel}{2}(A-1)(\hat{E}\hat{P}^*+\hat{E}^*\hat{P}) ,\end{aligned} \tag{5}$$

where A and B are the normalized values of the dc component of the population inversion and the modulation amplitude, respectively, which are the relevant control parameters:

$$A\equiv D^{(0)}/D_{\rm th} , \tag{6a}$$

$$B\equiv\zeta/D_{\rm th} . \tag{6b}$$

In the case of a very bad cavity (low-Q cavity), i.e.,

$$K\gg\gamma_\perp,\gamma_\parallel , \tag{7}$$

we can perform the adiabatic approximation for the field variable $\hat{E}(t)$. Thus the electric field follows adiabatically the atomic polarization as

$$\hat{E}(t)\simeq\hat{P}(t) . \tag{8}$$

After the procedure of adiabatic elimination, the resulting two-dimensional equations are

$$\frac{d}{dt}\hat{P}(t)=\gamma_\perp\hat{P}(\hat{D}-1) , \tag{9a}$$

$$\begin{aligned}\frac{d}{dt}\hat{D}(t)&=-\gamma_\parallel\hat{D}+\gamma_\parallel A+\gamma_\parallel B\cos(\omega_m t)\\ &\quad-\gamma_\parallel(A-1)|\hat{P}|^2 ,\end{aligned} \tag{9b}$$

which describe the temporal evolution of the material system. Here we divide the complex polarization $\hat{P}(t)$ into its amplitude $x(t)$ and phase $\theta(t)$, i.e., $\hat{P}(t)=x(t)\exp[i\theta(t)]$, and obtain

$$\frac{d}{dt}\theta(t)=0 , \tag{10a}$$

$$\frac{d}{dt}x(t)=\gamma_\perp x(\hat{D}-1) , \tag{10b}$$

$$\begin{aligned}\frac{d}{dt}\hat{D}(t)&=-\gamma_\parallel\hat{D}+\gamma_\parallel A+\gamma_\parallel B\cos(\omega_m t)\\ &\quad-\gamma_\parallel(A-1)x^2 .\end{aligned} \tag{10c}$$

These equations show that the phase of the polarization, which is nearly equivalent to that of the field due to Eq. (8), is constant in time even under the modulation of the population inversion. This is the characteristic feature of the resonant single-mode laser model with mean-field approximation.

Two first-order ordinary differential equations, (10b) and (10c), describing the magnitude of the polarization and the population difference, can be combined into one

second-order differential equation by eliminating the population difference as

$$\frac{d^2x}{dt^2}=\frac{1}{x}\left[\frac{dx}{dt}\right]^2-\gamma_{\parallel}\frac{dx}{dt}+\gamma_{\perp}\gamma_{\parallel}(A-1)x$$

$$+\gamma_{\perp}\gamma_{\parallel}Bx\cos(\omega_m t)-\gamma_{\perp}\gamma_{\parallel}(A-1)x^3 . \quad (11)$$

This shows that the external modulation is multiplicative. Therefore, in order to change this to the additive modulation, we introduce the logarithmic transformation

$$u(t)\equiv 2\ln|x(t)| . \quad (12)$$

This transform leads to the simple nonlinear equation of the oscillation. For the convenience of the following calculation, time is scaled by the period of the external modulation, i.e., $\tau\equiv\omega_m t$. Thus the fundamental equation is obtained as

$$\frac{d^2u}{d\tau^2}+k\frac{du}{d\tau}+6\bar{A}[\exp(u)-1]=\bar{B}\cos\tau , \quad (13)$$

where

$$k=\frac{\gamma_{\parallel}}{\omega_m} , \quad (14a)$$

$$\bar{A}=\frac{k\gamma_{\perp}}{3\omega_m}(A-1) , \quad (14b)$$

$$\bar{B}=\frac{2k\gamma_{\perp}}{\omega_m}B . \quad (14c)$$

Equation (13) is interpreted as describing the motion of a particle in the Toda potential $U(u)=\exp(u)-u-1$, with damping and with an external modulating force.[29-31] The Toda potential is shown in Fig. 1, which has a typical asymmetric curvature. The ratio k of the longitudinal relaxation constant $\gamma_{\parallel}$ to the modulation frequency ω_m is the damping constant of the Toda system, which is independent of the field intensity, contrary to Ref. 30. The normalized parameters $\bar{A}$ and $\bar{B}$ correspond to the strength of the nonlinearity of the Toda system and the magnitude of the modulation, respectively. Here we mention that the control parameters $\bar{A}$ and $\bar{B}$ are functions of the damping constant k and of the modulation frequency ω_m in addition to A and B, respectively. We pay attention to the case of $k>0$, $\bar{A}\geq 0$, and $\bar{B}\geq 0$ in this paper. Note here that we consider only the bad-cavity limit (7) and follow the whole dynamics of the material system (both the atomic polarization and the population difference). The condition for the rate-equation approximation, $\gamma_{\perp}\gg\gamma_{\parallel}$, is not required in our model. This point is different from Ref. 30, in which the rate equations were studied under both the conditions $K\gg\gamma_{\parallel}$ and $\gamma_{\perp}\gg\gamma_{\parallel}$.

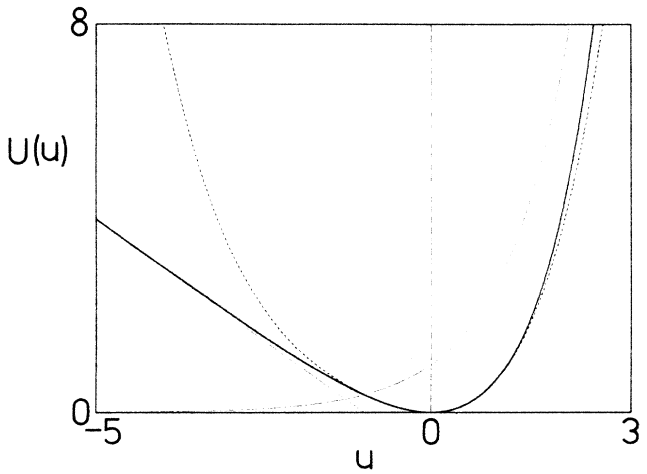

FIG. 1. Plot of the Toda potential $U(u)=\exp(u)-u-1$ (solid line). Dotted line is the truncated Toda potential $\bar{U}(u)=u^2/2+u^3/6+u^4/24$. The dot-dashed lines are the asymptotic forms of the Toda potential for large positive and large negative u.

The natural frequency of this system can be calculated in terms of the small oscillation around the minimum of the potential. The Toda potential is expanded around the minimum $u=0$ as

$$U(u)=\exp(u)-u-1 ,$$

$$=\frac{u^2}{2}+\frac{u^3}{6}+\frac{u^4}{24}+\cdots . \quad (15)$$

Therefore the frequency of the natural oscillation is

$$\omega_0\equiv(6\bar{A})^{1/2}=\frac{1}{\omega_m}[2\gamma_{\perp}\gamma_{\parallel}(A-1)]^{1/2} , \quad (16a)$$

which depends upon the dc component of the population inversion A. The relaxation frequency of the undriven system is calculated as

$$\omega_{\text{relax}}\equiv\left[6\bar{A}-\frac{k^2}{4}\right]^{1/2}$$

$$=\frac{1}{\omega_m}\left[2\gamma_{\perp}\gamma_{\parallel}(A-1)-\frac{\gamma_{\parallel}^2}{4}\right]^{1/2} , \quad (16b)$$

which exists only under the condition $A>1+\gamma_{\parallel}/8\gamma_{\perp}$. In the case of small longitudinal relaxation constant ($k=\gamma_{\parallel}/\omega_m\ll 1$) or large dc component of the population inversion, the relaxation frequency ω_{relax} coincides with the natural frequency ω_0. The nonlinear resonance phenomena around the natural frequency will be discussed in the second paper of a series.[27]

Equation (13) has a simple form. However, the existence of the damping term also induces several characteristics of the nonlinear dissipative dynamical system, e.g., chaos. The strong nonlinearity including the exponential term $\exp(u)$ and the nonautonomousness makes it impossible to obtain general and exact solutions of this equation. Therefore we employ numerical techniques to investigate this system extensively in Sec. III.

III. NUMERICAL RESULTS

In order to investigate the dependence of the dynamical properties of the Toda system (13) upon the control parameters $\bar{A}$ and $\bar{B}$, we make a numerical analysis also

in the case of strong modulation. The nonlinear second-order differential equation (13) is transformed to two first-order coupled differential equations,

$$\frac{dv}{d\tau} = -kv - 6\bar{A}[\exp(u) - 1] + \bar{B}\cos\tau \ , \tag{17a}$$

$$\frac{du}{d\tau} = v \ , \tag{17b}$$

to be solved by using a fourth-order Runge-Kutta-Gill routine with double precision. This method is effective in avoiding the accumulation of the round-off errors. In order to eliminate troubles due to the numerical divergence, we employ the method of integration along the solution arc (the automatic control of the time increments for the integration). The following results are independent of the increment for the integration in the case of a fairly small one.

We perform the numerical calculation in the two cases of the ratio $k = \gamma_\parallel/\omega_m$, i.e., $k = 1.0$ and 0.1. In Sec. III A the numerical results in the $k = 1.0$ case are presented. This corresponds to the situation $\omega_m = \gamma_\parallel$. In addition, we consider the situation $\gamma_\parallel = 0.5\gamma_\perp$ in order to satisfy the condition $\omega_m = 0.5\gamma_\perp < \gamma_\perp$, as shown in Sec. II. These parameters are chosen to be same as that of the multimode laser system investigated in Refs. 8 and 9. On the other hand, the case of $k = 0.1$ is examined in Sec. III B. This situation can be realized by choosing the parameters, e.g., as $\gamma_\parallel = 0.05\gamma_\perp$ and $\omega_m = 10.0\gamma_\parallel$, satisfying the condition $\omega_m < \gamma_\perp$. Thus the two cases $k = 1.0$ and $k = 0.1$ correspond to the cases of large and small longitudinal relaxation constant, respectively.

A. The fast population relaxation case ($k = \gamma_\parallel/\omega_m = 1.0$)

In the $k = 1.0$ case, the dependence of two control parameters $\bar{A}$ and $\bar{B}$ upon A and B is calculated as

$$\bar{A} = \tfrac{2}{3}(A - 1) \ , \tag{18a}$$

$$\bar{B} = 4B \ . \tag{18b}$$

We vary the control parameters in the regions $\bar{A} \in [0, 2.5]$ and $\bar{B} \in [0, 20]$, which are equivalent to $A \in [1, 4.75]$ and $B \in [0, 5]$, respectively. These are reasonable for comparing with the results of the multimode laser system.[8,9]

The phase diagram of the Toda system is obtained as a function of two control parameters $\bar{A}$ and $\bar{B}$, as shown in Fig. 2. The numbers therein stand for the fractions of the modulation frequency, that is, the harmonic oscillation is denoted by 1 and the subharmonic oscillation of order $\frac{1}{2}$ (period-2 motion) as $\frac{1}{2}$. Thus the period-n oscillation is denoted as $1/n$. Both symbols C and I represent chaotic behaviors which show different time evolutions. Region C shows the *quasiperiodic chaos* and region I is the *intermittent kicked chaos*, which are investigated in detail afterwards. In the region of the harmonic oscillations denoted by 1, the Toda system behaves sinusoidally in accordance with the external modulation. Corresponding dynamics of the laser emission is an ordered spiking pulse train. Two oscillations of the harmonic and the subharmonic occupy the main regions toward the chaotic region.

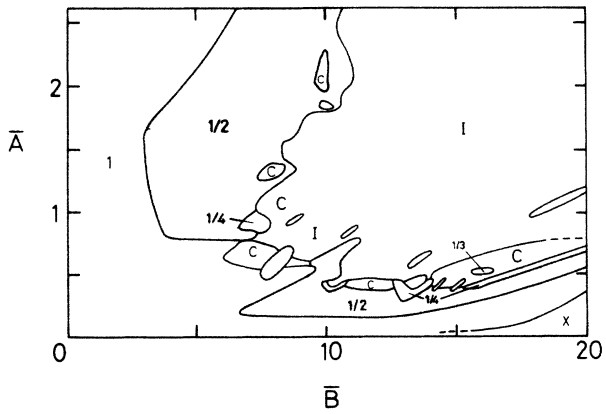

FIG. 2. Phase diagram of modulation characteristics under the condition $k = \gamma_\parallel/\omega_m = 1.0$ in two-dimensional parameter space: $\bar{A}$ and $\bar{B}$, corresponding to $A \in [1, 4.75]$ and $B \in [0, 5]$. The numbers stand for the fractions of the modulation frequency. The subharmonic oscillation of order $\frac{1}{2}$ (the period-2 motion) is observed in the dark regions. In the C and I regions, the system exhibits chaos with different characteristics. The boundary between the C and I regions is ambiguous. This phase diagram is coarse grained, and a realistic diagram is filled with finer structure shown in the bifurcation diagrams (e.g., Figs. 3–9).

In the region of $\bar{A} < 0.35$, chaos is not observed at all in this system even under the strong modulation. The characteristic feature in the small-$\bar{A}$ region ($\bar{A} < 0.35$) is that the Toda particle cannot oscillate near the potential minimum $u = 0$ at large modulation amplitude ($\bar{B} > 16$), which region is denoted as $\times$ in the phase diagram. The Toda particle goes away from the origin to the negative direction ($u \to -\infty$). This breakdown phenomenon is equivalent to the no emission of the laser ($\hat{E} \to 0$). This results from the fact that the buildup of the laser emission cannot pursue the modulation of the pumping in the region of small $\bar{A}$ and large $\bar{B}$.

In the left-low (small-$\bar{A}$ and -$\bar{B}$) region of the diagram ($k = 1.0$), no subharmonic oscillation can be observed. However, for $\bar{A} \geq 0.8$, the harmonic oscillation is bound to bifurcate to the subharmonic oscillation of order $\frac{1}{2}$. This subharmonic state loses its stability to show quasi-periodic or chaotic motions as increasing with modulation amplitude $\bar{B}$.

The bifurcation diagrams as a function of the modulation amplitude $\bar{B}$ are shown in Figs. 3–9 for several values of $\bar{A}$. These diagrams are obtained by plotting the maximum and minimum points of time evolutions $u(\tau)$ at each parameter $\bar{B}$. In these diagrams, the harmonic oscillation is represented by two points corresponding to its maximum and minimum. Chaotic oscillation corresponds to the region with many dots. The particle in the Toda potential gradually shifts to the negative direction as $\bar{B}$ increases. This comes from the asymmetric curvature of the Toda potential with linear dependence on the displacement u in the $u < 0$ region. In the $u > 0$ region, the particle is subject to the strong repulsive force due to the hard wall of the potential $\exp(u)$, and cannot move to the positive region. Therefore the upper bound of u

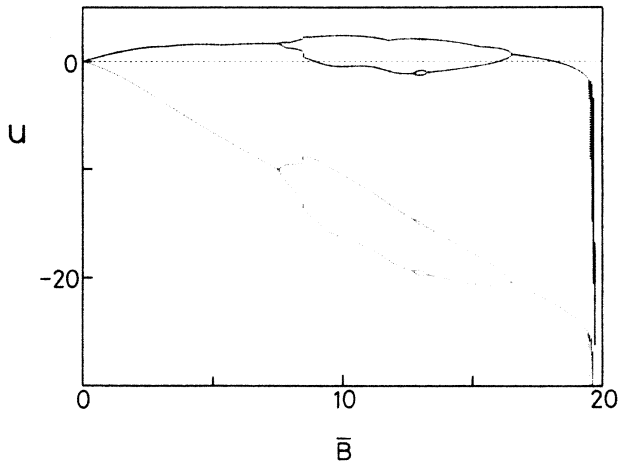

FIG. 3. Bifurcation diagram of u against the modulation amplitude $\bar{B}$ for $k=1.0$ and $\bar{A}=0.3$. The incomplete period-doubling sequence is observed.

seems to exist in the bifurcation diagrams.

For $\bar{A}=0.3$ (Fig. 3), the bifurcation diagram shows the typical *incomplete* period-doubling sequence which is terminated by the breakdown at $\bar{B}=19.3$ The harmonic and the subharmonic oscillations of order $\frac{1}{2}$ and $\frac{1}{4}$ are observed. The harmonic solution changes to the subharmonic one in the period-doubling sequence via the saddle-node bifurcation. The harmonic oscillation is revived at the stronger modulation amplitude after the inverse bifurcations. We also find the discontinuous jump in the subharmonic state. On the other hand, for $\bar{A}=0.4$, the subharmonic oscillation of order $\frac{1}{2}$ is found to change discontinuously to the unstable quasiperiodic state at $\bar{B}=9.45$, as shown in Fig. 4. This develops into the quasiperiodic chaos with many characteristic windows. At large $\bar{B}$, the inverse period-doubling bifurcation occurs again to exhibit harmonic oscillation.

In the case of $\bar{A}=0.6\sim0.7$, the regions of the period-2 oscillation are very small or vanish. The harmonic oscil-

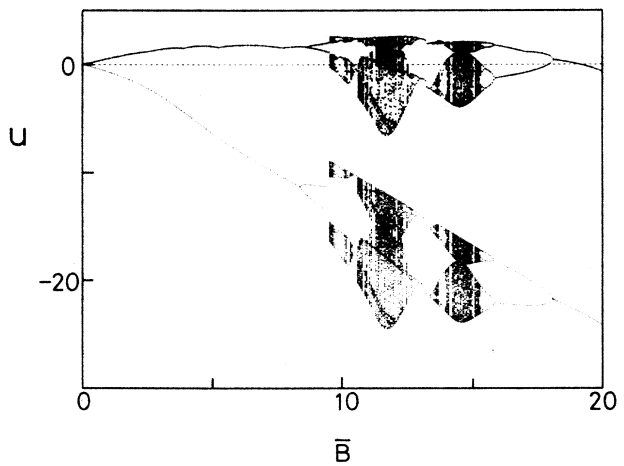

FIG. 4. Bifurcation diagram of u for $k=1.0$ and $\bar{A}=0.4$.

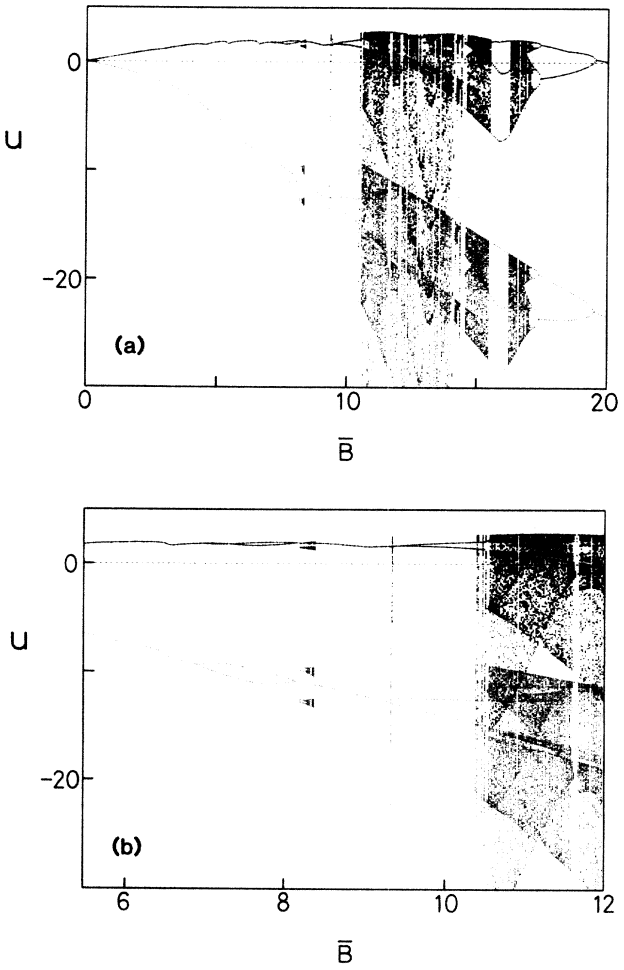

FIG. 5. (a) Bifurcation diagram of u for $k=1.0$ and $\bar{A}=0.5$. (b) Enlargement of the region of the onset of chaos. The catastrophic change to chaos is observed at $\bar{B}=10.5$.

lation seems to change directly into the quasiperiodic or the chaotic state, as shown in Fig. 6(a). This results from the instability of the harmonic oscillation. The corresponding bifurcation diagram of the amplitude of the laser emission $|\hat{E}|=\exp(u/2)$ is given in Fig. 6(b). For $\bar{A}=0.9$ (Fig. 8), we can easily find the instability of the subharmonic oscillation (of order $\frac{1}{4}$) resulting in the unstable quasiperiodic motion at $\bar{B}=7.2$. This quasiperiodic instability develops into the quasiperiodic chaos which is terminated by the noisy period-3 window (at $\bar{B}=7.6$). Subsequently, the intermittent kicked chaos appears. This scenario is true of the $\bar{A}=0.9\sim1.3$ case (see Fig. 9).

We find from the bifurcation diagrams that there are two kinds of onset of chaos as the modulation amplitude $\bar{B}$ increases: One is due to the *quasiperiodic instability* and the other is due to the *catastrophic crisis*.[32,33] These two onsets of chaos are dependent upon the control parameter $\bar{A}$. The former is a continuous path to chaos fully developed in the strong modulation, as observed, e.g., in the case of $\bar{A}=0.7$, 0.9, and 1.3 (see Figs. 6, 8, and 9). The harmonic oscillation changes into the subharmonic

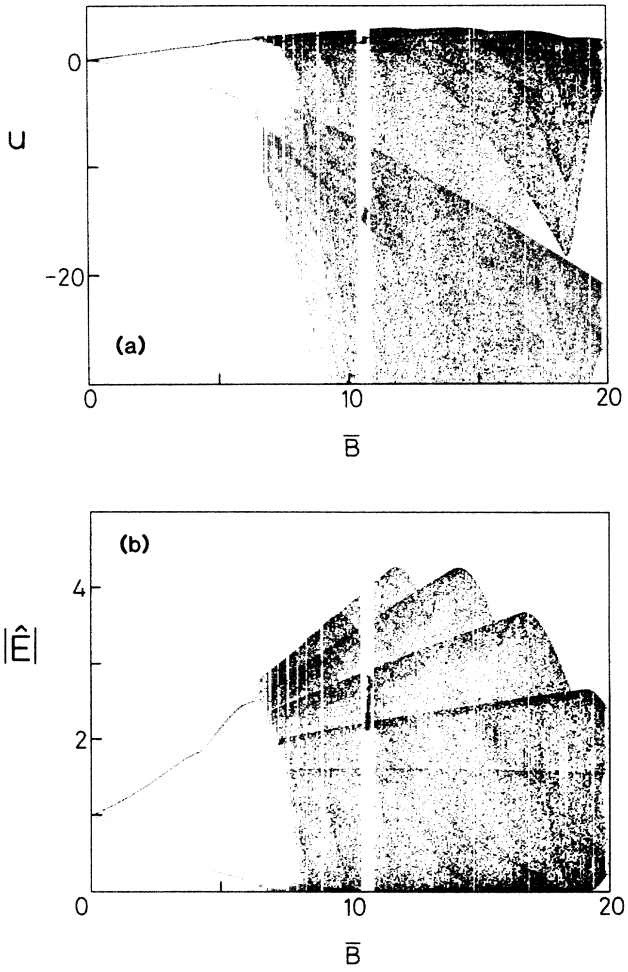

FIG. 6. (a) Bifurcation diagram of u for $k=1.0$ and $\bar{A}=0.7$. The harmonic oscillation yields the quasiperiodic instability at $\bar{B}=6.5$. (b) The corresponding bifurcation diagram of the amplitude of the field $|\hat{E}|$.

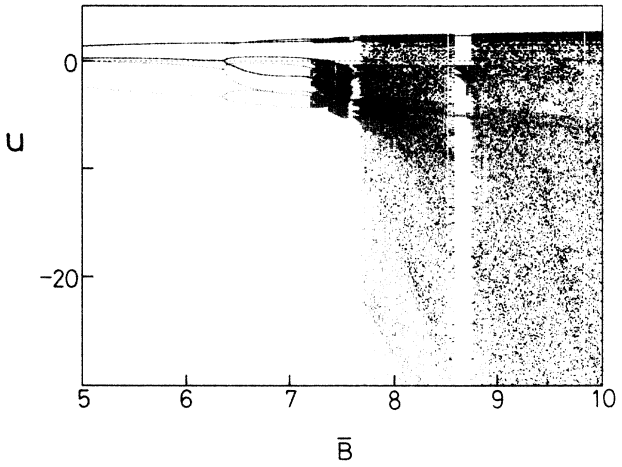

FIG. 8. Bifurcation diagram of u for $k=1.0$ and $\bar{A}=0.9$.

oscillation via the (incomplete) period-doubling bifurcations. In this sequence, both the harmonic and the subharmonic oscillations yield the quasiperiodic instabilities resulting in the chaotic oscillations as $\bar{B}$ increases. The quasiperiodic route to chaos is confirmed in the power spectrum by the peaks at incommensurate frequencies to the modulation frequency (Fig. 10). This is a multidimensional characteristic mechanism of the onset of chaos in the modulated nonlinear system. In addition to this, another kind of onset of chaos is observed. The latter is one of discontinuous (catastrophic) paths to chaos, which is the abrupt change to chaotic motion as the parameter $\bar{B}$ is varied; for example, at $\bar{A}=0.5$ and $\bar{B}=10.38$ in Figs. 5(a) and 5(b) or at $\bar{A}=0.8$ and $\bar{B}=7.6$ in Fig. 7. This occurs when the unstable periodic orbit just touches the chaotic band attractor. There is also evidence in the bifurcation diagram that the density of attractor points in the large attractor near the crisis concentrates in the bands, and gradually spreads out. These

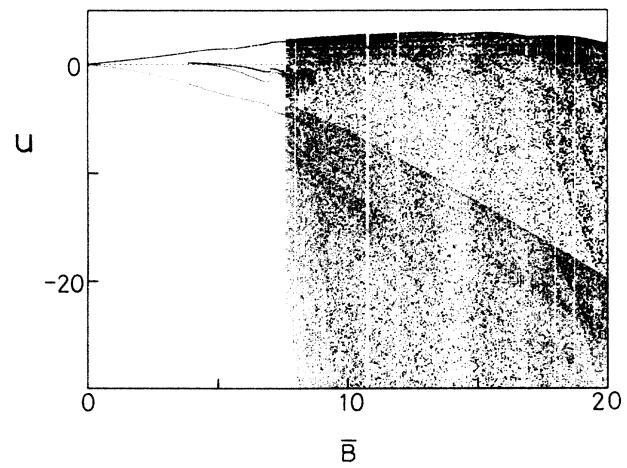

FIG. 7. Bifurcation diagram of u for $k=1.0$ and $\bar{A}=0.8$.

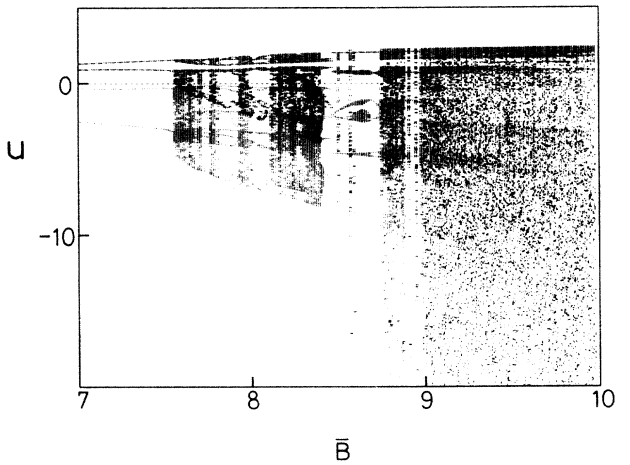

FIG. 9. Enlargement of the bifurcation diagram of u for $k=1.0$ and $\bar{A}=1.3$.

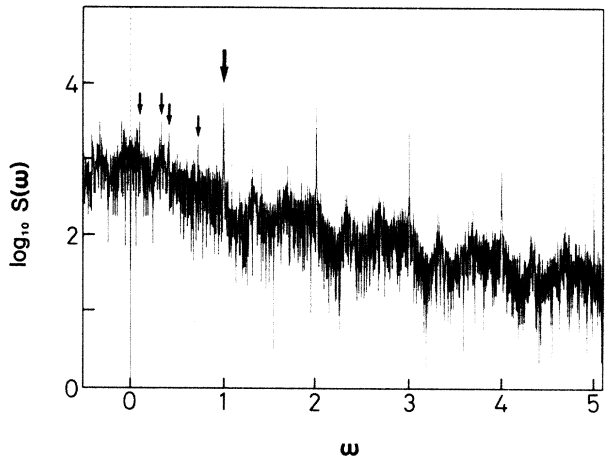

FIG. 10. Spectral density of the unstable quasiperiodic state, i.e., $k=1.0$, $\overline{A}=0.9$, and $\overline{B}=7.3$. The large arrow indicates the fundamental frequency component of the external modulation. Incommensurate (quasiperiodic) frequencies are denoted by smaller arrows. The sum and difference frequency components among them are also observed. The frequency is scaled by the external modulation frequency.

two routes to chaos suggest that several attractors, including the strange one, coexist and that their relations are sensitive to the parameter $\overline{A}$.

There are periodic windows with odd fractions of the modulation frequency, i.e., ω_m/n $(n=3,5,6,7,\ldots)$, denoted as $1/n$ within the region of chaos. In these windows, the subharmonic oscillations of order $\frac{1}{3}$ and $\frac{1}{6}$ are found to be sustained, which are characteristics of the nonlinear dynamical system yielding chaos. This typical period-3 window comes from tangent or saddle-node bifurcation, which also creates a period-3 unstable orbit. The period-$\frac{3}{2}$ motion is also observed. Figure 11 is the power spectral density $S(\omega)$ of $u(\tau)$ in the period-6 window in the semilog frame. This state corresponds to the subharmonic state of the period-3 oscillation.

There are two kinds of chaos in a forced Toda system denoted as C and I in the phase diagram (Fig. 2). The typical time evolution of chaos in the C regions is shown in Fig. 12(a). The fundamental period of oscillation coincides with that of the modulation. However, the values of local peaks are very random and chaotic. This kind of chaos can be observed in the vicinity of the regions of quasiperiodic oscillations. We will hereafter call this the

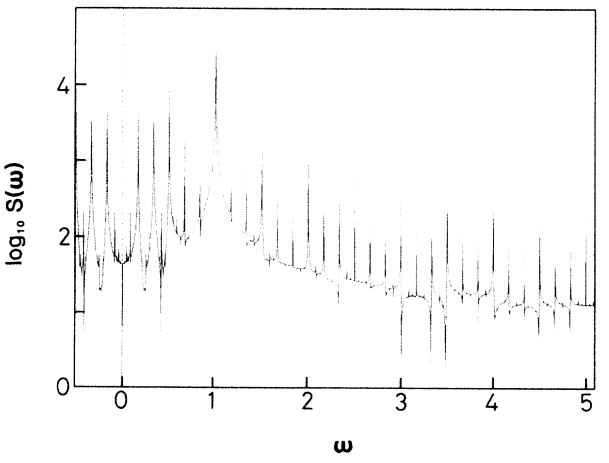

FIG. 11. Power spectral density of the subharmonic oscillation of order $\frac{1}{6}$ (the period-6 motion) in the $k=1.0$, $\overline{A}=0.4$, and $\overline{B}=15.035$ cases.

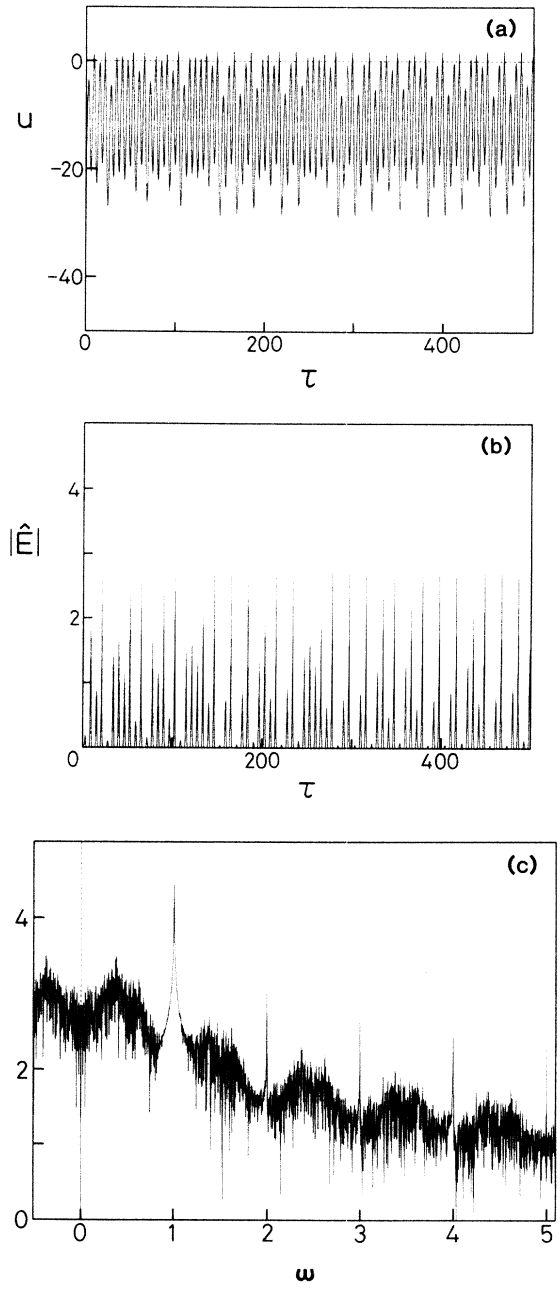

FIG. 12. (a) Typical time evolution of the quasiperiodic chaos in $k=1.0$, $\overline{A}=0.6$, $\overline{B}=18.0$. (b) Corresponding emission of the laser. (c) Power spectral density of the quasiperiodic chaos. The noisy background and the modulation peaks coexist.

quasiperiodic chaos. The amplitude $u(\tau)$ is bounded in a region about $-28.0 \leq u \leq 2.0$ The corresponding laser emission is a spiking pulse train with random fluctuations of the peak powers, as shown in Fig. 12(b). In the chaotic region, there are several maximum amplitudes of the chaotic emission, as shown, e.g., in Fig. 6(b). The maximum intensity of chaotic light changes abruptly as a function of the modulation amplitude. The power spectral density shows a broad noisy background with modulation peaks [Fig. 12(c)]. Some structures of background and quasiperiodic components are also observed.

We have calculated the return map[25,26] (one-dimensional transfer function) from the sequence each of the maximum and the minimum points of the time evolutions $u(\tau)$ by use of the Lorenz plot.[10] The quasiperiodic chaos has well-defined mapping functions as shown in Figs. 13(a) and 13(c). It has a smooth curve with a single peak similar to the logistic map $u \rightarrow au(1-u)$, with $0 \leq a \leq 4$. Thus the quasiperiodic chaos in the forced Toda system is found to be well described by the one-dimensional map. Figure 13(a) shows that the return map has an approximate closed-loop structure in a region of $u_n \in [-23.5, -19.0]$. This comes from the torus structure of the attractor of the quasiperiodic motion. The invariant probability measure of these map functions has been calculated, too, as shown in Figs. 13(b) and 13(d). The invariant measure of the map function is defined as the time average of the Dirac δ's at the point u,

$$\mu(u) \equiv \lim_{N \rightarrow \infty} \left[\frac{1}{N} \sum_{i=0}^{N-1} \delta(u - F^{(i)}(u_0)) \right], \tag{19}$$

where $F^{(i)}(u)$ is the ith iterated map function and u_0 the fixed point. This probability measure describes how frequently various parts of the attractor are visited by the orbit describing the system. The measure is invariant under the dynamical system, i.e., invariant under time evolution. The singular structures can be seen as δ-function-like peaks, which are a characteristic feature of low-dimensional dynamical systems. They reflect the singular ergodic measure of the attractors. The invariant measure of the map constructed by the minimum points in this case [Fig. 13(b)] is similar to that of the logistic map for the parameter $a = 3.678\,57\ldots$ with square-root singularities.[25]

Here we must also pay attention to the some differences from the results originating in the one-dimensional mapping function. If the one-dimensional map has the unimodal shape of the logistic map, then a typical control takes the dynamical system through a sequence of successive flip bifurcations. However, incomplete sequences of period doubling can be observed in this Toda system as shown, for example, in Fig. 3. Such interrupted cascades become possible most notably when Poincare mapping cannot be summarized by a one-dimensional map. Therefore our forced Toda system cannot be reduced to a one-dimensional map in a precise sense. This fact is reflected in the Lorenz plot as the multivalued nature, as shown in Fig. 13(a). The higher-dimensional properties and the continuous time character

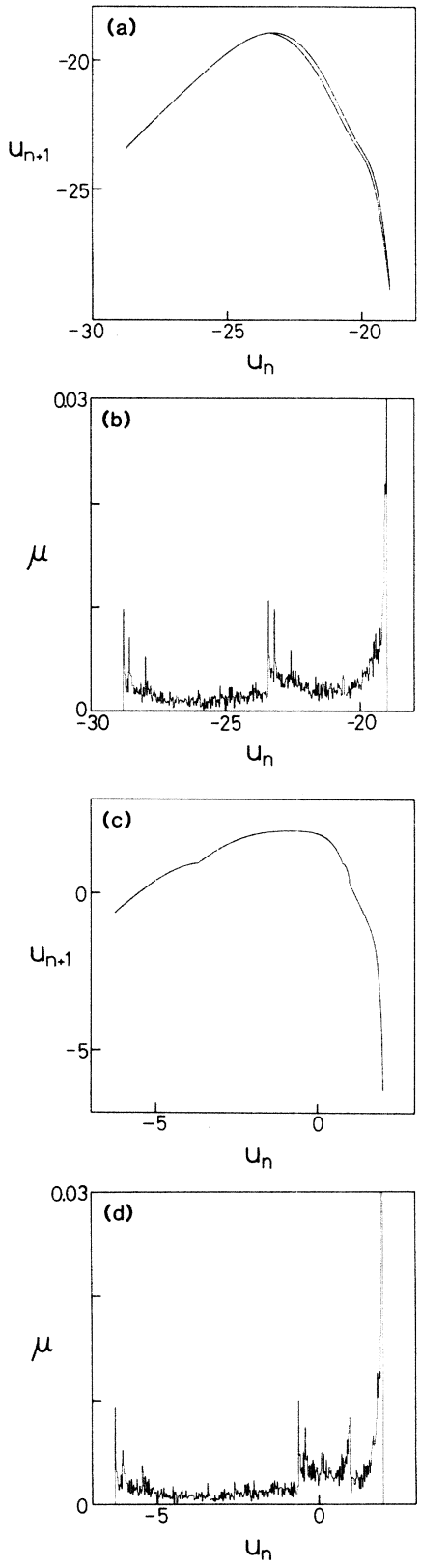

FIG. 13. (a) Return map of the successive local minima of the time evolution $u(\tau)$. Closed-loop structure can be seen. (b) Invariant probability measure of the map function (a). u_n is divided into 450 bins. (c) Return map of the successive local maxima of the time evolution $u(\tau)$. (d) Invariant probability measure of the map function (c).

of the differentiable dynamical system (in the *differential* equation, not in the *difference* equation) play roles in these facts.

In the regions of the fully developed quasiperiodic chaos, chaotic motions with small sub- or higher-periodic components are also observed. Figure 14(a) describes the power spectral density of the quasiperiodic chaos with a nearly period-7 component. This period-7 component almost works as a quasiperiodic component. From this chaos, one-dimensional maps are constructed [Figs. 14(b) and 14(c)], which have several maxima different from the logistic map. The map of the minimum points is smooth but has a multivalued structure with a subpeak, and the map function of the maximum one is not smooth with several local peaks. Their invariant measures are also singular. Chaos with the higher-harmonic component are also obtained. The second-harmonic oscillation in addition to the subharmonics is superposed in chaotic oscillation as shown in Fig. 15(a). The second-harmonic frequency component is larger in the power spectrum [Fig. 15(b)] than the harmonic component.

The chaos in region I has a typical time evolution, including the intermittency as shown in Fig. 16(a). We call this the *intermittent kicked chaos.* The amplitude $u(\tau)$ is kicked intermittently to a large negative value by the modulation and gradually comes back to the potential minimum $u=0$ with a slight modulation. In these regions, laser emits light pulses intermittently as shown in Fig. 16(b). The power spectrum [Fig. 16(c)] has a broad noisy profile with peaks of the modulation component.

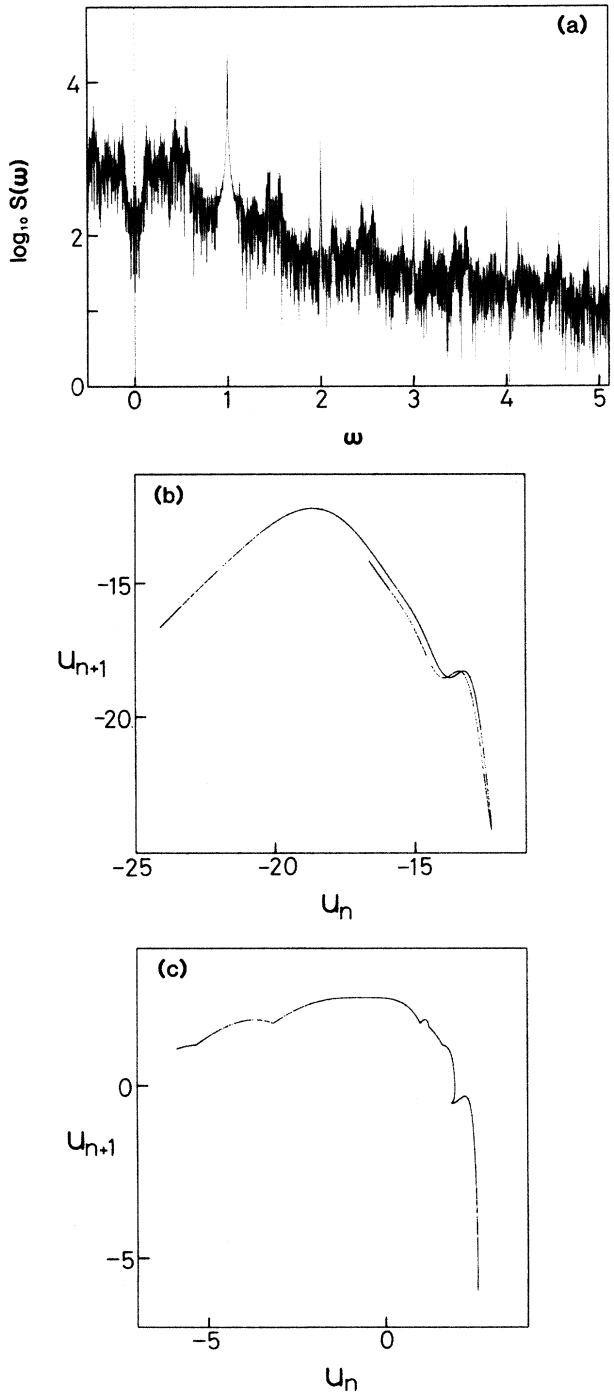

FIT. 14. (a) Power spectral density of the period-7 chaos in the case of $k=1.0$, $\overline{A}=0.4$, and $\overline{B}=12.0$. (b) Return map of the successive local minima of $u(\tau)$. The multipeaked and the multivalued characters are observed. (c) Return map of the successive local maxima of $u(\tau)$.

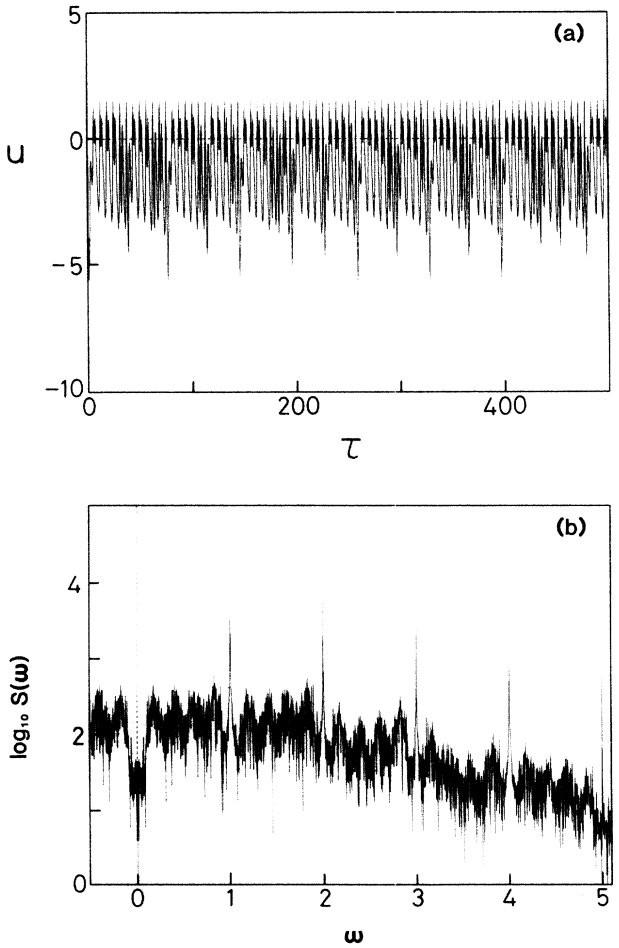

FIG. 15. (a) Quasiperiodic chaos with the period-5 and the second-harmonic components for $k=1.0$, $\overline{A}=1.3$, and $\overline{B}=7.7$. (b) Power spectral density. The second-harmonic frequency is dominant.

These kicks to the negative direction are due to the external modulation and the asymmetric line shape of the Toda potential $U(u)=\exp(u)-u-1$, which is equivalent to the system with a very hard spring in $u>0$ region and a very soft spring in $u<0$ region. This intermittent kicked chaos cannot be summarized by one-dimensional maps. The well-defined smooth map functions cannot be obtained from the local maxima and minima by the Lorenz plot, contrary to the case of quasiperiodic chaos. The intermediate state from quasiperiodic to intermittent kicked chaos is also observed (Fig. 17).

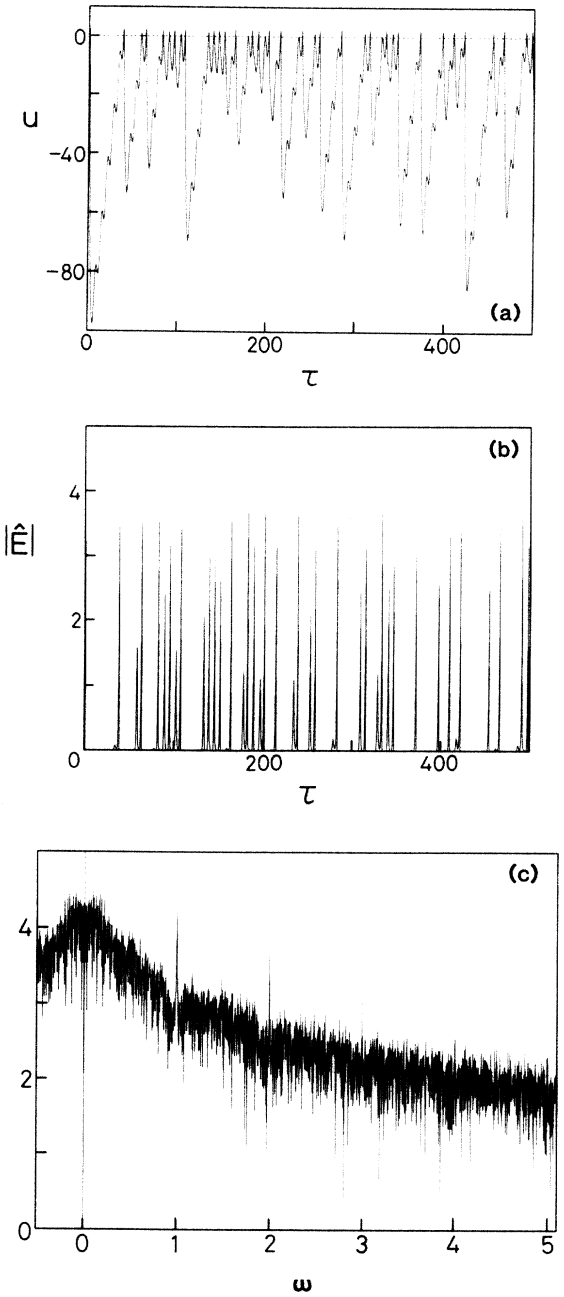

FIG. 16. (a) Intermittent kicked chaos in $k=1.0$, $\bar{A}=0.9$, and $\bar{B}=10.0$. (b) Corresponding emission of the laser. Intermittent pulsing is a characteristic of this chaos. (c) The power spectral density of the intermittent kicked chaos.

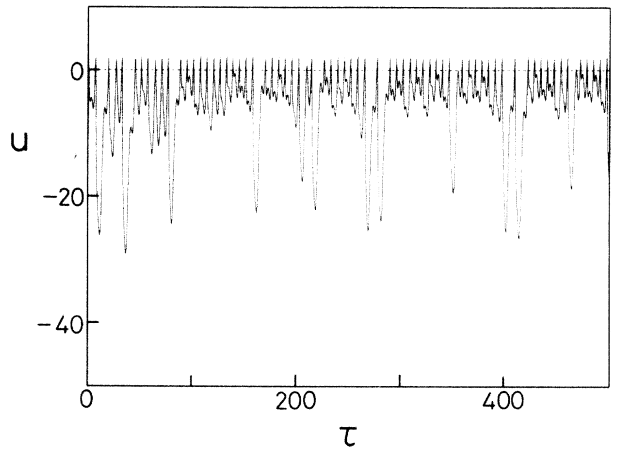

FIG. 17. Transient state from the quasiperiodic to the intermittent kicked chaos in $k=1.0$, $\bar{A}=0.9$, and $\bar{B}=8.0$.

B. The slow population relaxation case ($k=\gamma_{\parallel}/\omega_m=0.1$)

In this case of $k=0.1$, the dependence of $\bar{A}$ and $\bar{B}$ upon A and B is described as

$$\bar{A}=\tfrac{1}{15}(A-1)\,, \tag{20a}$$

$$\bar{B}=\tfrac{2}{5}B\,. \tag{20b}$$

In this section, we vary the above two control parameters in the following regions: $\bar{A}\in[0,0.32]$ and $\bar{B}\in[0,4]$, which are equivalent to $A\in[1,5.8]$ and $B\in[0,10]$, respectively.

As shown in Fig. 18, the phase diagram has a complicated structure with several periodic windows. There are

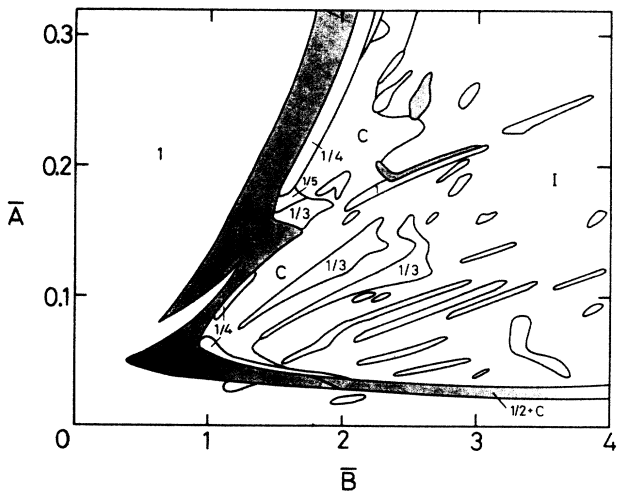

FIG. 18. Phase diagram of modulation characteristics under the condition $k=0.1$ in the two-dimensional parameter space $\bar{A}$ and $\bar{B}$, corresponding to $A\in[1,5.8]$ and $B\in[0,10]$. The subharmonic oscillation of order $\frac{1}{2}$ is observed in the dark regions. The islandlike structure is due to the several periodic windows. This phase diagram is also coarse grained.

the regions of harmonic oscillation (denoted by 1) and of subharmonic oscillation of order $1/n$ (denoted by $1/n$) on the way to quasiperiodic chaos. The subharmonic oscillations of order $\frac{1}{2}$ are dominant in the region to chaos. However, higher-order bifurcations in the period-doubling sequence, in particular, the subharmonics of order $\frac{1}{4}$ are clearly observed.

Subharmonic oscillations of order $\frac{1}{2}$ exist in the left-low region (small $\overline{A}$ and $\overline{B}$) of the phase diagram, different from the case of $k=1.0$. In the case of $\overline{A}<0.02$, only periodic oscillations are observed and chaos is not. In the $\overline{A}>0.02$ region, two kinds of chaos exist resulting from the quasiperiodic instability of subharmonic oscillations. The complete period-doubling sequences are also observed in contrast to the case of $k=1.0$. The many-periodic windows exist to show chaotic and periodic regions alternately. These coincide with the results of Ref. 23. These complex behaviors showing the periodic windows are a characteristic of the nonlinear system yielding chaos.

As is similar to the case of $k=1.0$, two kinds of chaos are observed: quasiperiodic chaos and intermittent kicked chaos. The former one can be well approximated by one-dimensional mapping by constructing the Lorenz plot of the time evolution. The invariant measure of this map function is singular, resulting in the δ-functionlike peaks.

For $\overline{A}=0.05$ (Fig. 19), the period-doubling bifurcation is clearly observed, and results in quasiperiodic motion and quasiperiodic chaos. In the $\overline{B}>1.6$ case, the system shows alternately the intermittent kicked chaos and the periodic windows as $\overline{B}$ increases. The abrupt increase of the amplitude of the harmonic oscillation is observed at $\overline{A}=0.08$ and $\overline{B}=0.65$, corresponding to the point of the cyclic fold, as shown in Fig. 20. This jump at the cyclic fold suggests the hysteresis phenomenon. For the region of $0.09\leq\overline{A}\leq 0.12$ (see, e.g., Fig. 21), we find from the bifurcation diagrams that the subharmonic oscillation of order $\frac{1}{2}$ lies between the harmonic oscillations. Figure 22

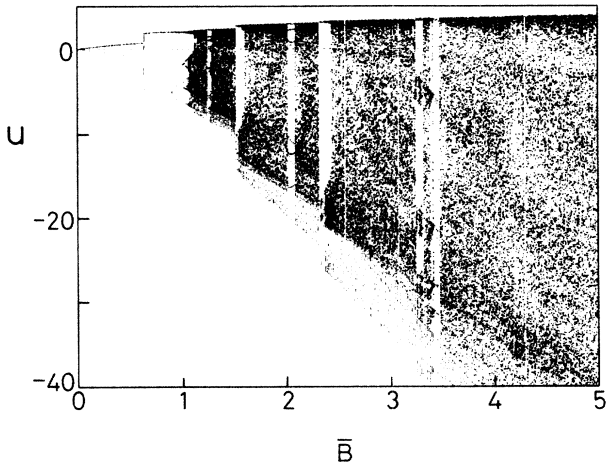

FIG. 20. Bifurcation diagram of u for $k=0.1$ and $\overline{A}=0.08$.

($\overline{A}=0.18$ case) also shows a revival of harmonic oscillation after the period-doubling cascade, the quasiperiodic and chaotic regions with windows. Harmonic oscillation changes abruptly into intermittent kicked chaos via the catastrophic crisis. In this way, the subharmonic oscillation of order $\frac{1}{2}$ can be observed in the $k=0.1$ case, even under the small-$\overline{A}$ condition. By increasing the modulation amplitude $\overline{B}$, harmonic oscillation comes out again after the subharmonic states. This is a characteristic of this system in a small-k case and will be investigated in a following paper.[27]

In the $\overline{A}=0.03$ case, the system shows a strange bifurcation diagram, as shown in Fig. 23. Harmonic oscillation bifurcates to the period-2 motion via the subharmonic saddle-node bifurcation at $\overline{B}=2.0$. The higher-order subharmonics, i.e., the order of $1/n$ ($n=4,8,16,32,\ldots$), are not observed. However, the subharmonic oscillation of order $\frac{1}{2}$ loses its stability, depending sensitively upon

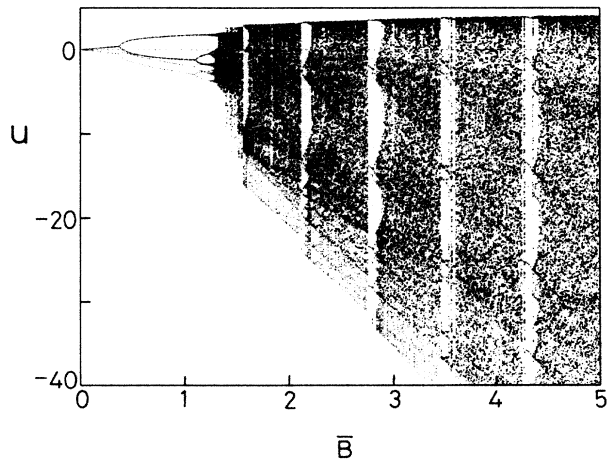

FIG. 19. Bifurcation diagram of u against the modulation amplitude $\overline{B}$ for $k=0.1$ and $\overline{A}=0.05$.

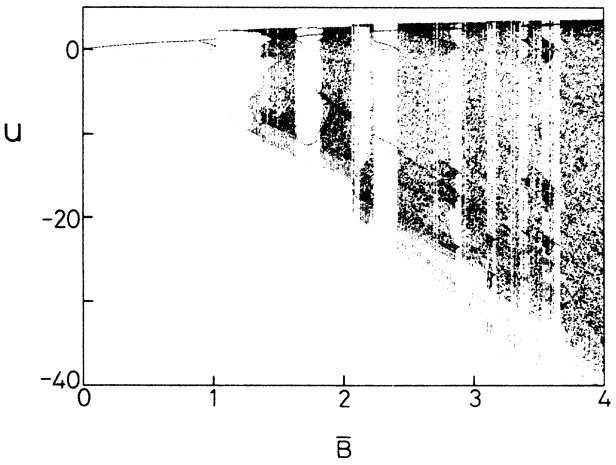

FIG. 21. Bifurcation diagram of u for $k=0.1$ and $\overline{A}=0.11$.

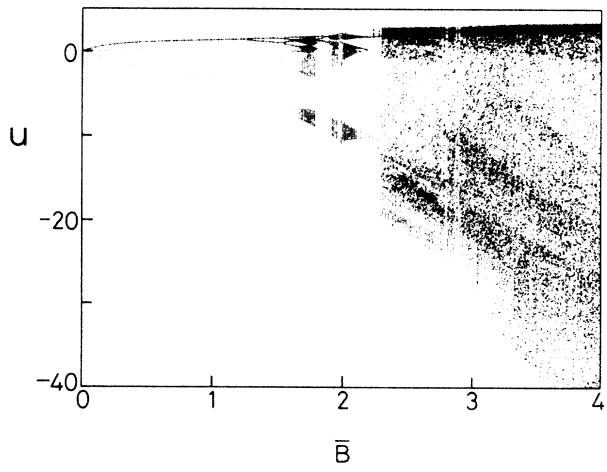

FIG. 22. Bifurcation diagram of u for $k=0.1$ and $\bar{A}=0.18$.

the control parameter $\bar{B}$ to show the alternate structure of the period-2 oscillation and chaos. In the harmonic oscillation, the period-3 and the period-6 motions occur in a small region $\bar{B}\in[1.13,1.30]$, with discontinuous jumps. This suggests the existence of hysteresis or isolas.

In both cases of $k=1.0$ and 0.1, the quasiperiodic instability of the subharmonic and the harmonic oscillations is found to play a key role in inducing chaos in this modulated system, which will also be shown in the analytic studies.[27] The intermittent kicked chaos is due to the extremely asymmetric potential in the modulated system. In Sec. IV, we investigate by a simple discrete model the effect of the asymmetry of a Toda potential on yielding chaos, having a one-dimensional mapping structure.

IV. HARD-WALL MODEL

As shown in the Lorenz plot in Sec. III, the quasiperiodic chaos in a Toda system (C regions in the phase diagrams) have well-defined one-dimensional map functions. This means that the chaotic dynamics of the quasiperiodic chaos can be summarized by the one-dimensional (return) map. Complex chaotic behavior in the coupled ordinary differential equation (ODE) system results partially from the simple discrete map in one dimension.

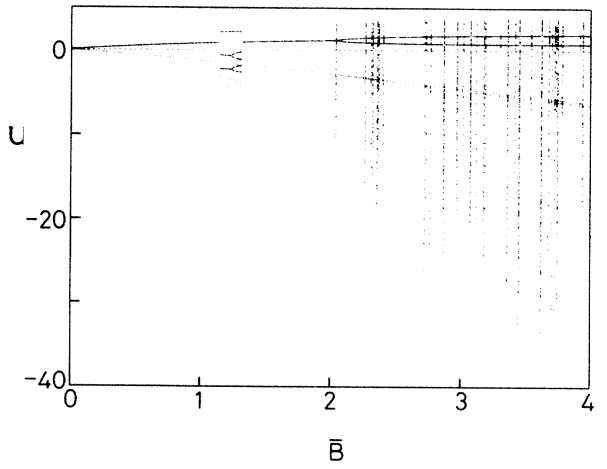

FIG. 23. Bifurcation diagram of u for $k=0.1$ and $\bar{A}=0.03$.

In this section we derive an analytical expression of the one-dimensional map which characterizes the dynamics of a Toda system for the mathematical studies on probability measure and bifurcation sequence. Moreover, the effect of the strong repulsive force resulted from the asymmetric potential is also examined by the hard-wall potential model employed in this section.

The Toda potential $U(u)=\exp(u)-u-1$ has an extremely asymmetric curvature. It has a linear dependence on the displacement u in the $u<0$ region:

$$\lim_{u\to-\infty} U(u)=-u-1 , \tag{21}$$

which is equivalent to free fall. On the other hand, the system contains a very hard spring in $u>0$ region,

$$\lim_{u\to\infty} U(u)=\exp(u) . \tag{22}$$

This works as a strong repulsive force, just as a hard wall at $u=0$. In this section we approximate a Toda potential as a simple hard-wall potential to derive one-dimensional recursion relations. In addition, chaos is shown to exist also in this map.

The Toda potential is assumed to be approximated as a simpler potential, i.e.,

$$U(u)=\begin{cases}\infty, & u>0\\ -u, & u\le 0 .\end{cases} \tag{23}$$

The particle in this potential cannot go into the region $u>0$ because of the infinitely high potential barrier. In the $u\le 0$ region, the motion of the particle is the free fall described by

$$\frac{d^2u}{d\tau^2}+k\frac{du}{d\tau}-6\bar{A}=\bar{B}\cos\tau . \tag{24}$$

This is solved easily as

$$u(\tau)=\frac{6\bar{A}}{k}\tau-\frac{C_1}{k}\exp(-k\tau) -\frac{\bar{B}}{(1+k^2)^{1/2}}\cos(\tau+\theta)+C_2 , \tag{25}$$

where

$$\theta=\arctan k , \tag{26a}$$

$$C_1=\dot{u}_0-\frac{6\bar{A}}{k}-\frac{k}{1+k^2}\bar{B} , \tag{26b}$$

$$C_2=u_0+\frac{\dot{u}_0}{k}-\frac{6}{k^2}\bar{A} , \tag{26c}$$

with initial conditions $u(\tau=0)=u_0$ and $\dot{u}(\tau=0)=\dot{u}_0$. The particle moves to the origin $u=0$ with modulating motion and collides with the infinitely high barrier at

$u=0$. It is perfectly reflected by the hard wall to the opposite direction ($u<0$) and comes back again to the wall after a certain time.

The time interval τ_n between the $(n-1)$th and the nth collision is determined, according to (25), by the recursion relations for $n=1,2,3,\ldots$, i.e.,

$$\frac{6\bar{A}}{k}\tau_n-\frac{C_1^{(n-1)}}{k}\exp(-k\tau_n)-\frac{\bar{B}}{(1+k^2)^{1/2}}\cos(\tau_n+\theta)+C_2^{(n-1)}=0\ , \quad (27)$$

where

$$C_1^{(n-1)}=-\dot{u}_{n-1}-\frac{6\bar{A}}{k}-\frac{k}{1+k^2}\bar{B}\ , \quad (28a)$$

$$C_2^{(n-1)}=-\frac{\dot{u}_{n-1}}{k}-\frac{6}{k^2}\bar{A}\quad (n=2,3,4,\ldots)\ , \quad (28b)$$

and

$$C_1^{(0)}=\dot{u}_0-\frac{6\bar{A}}{k}-\frac{k}{1+k^2}\bar{B}\ , \quad (28c)$$

$$C_2^{(0)}=u_0+\frac{\dot{u}_0}{k}-\frac{6}{k^2}\bar{A}\ . \quad (28d)$$

Here, $\dot{u}_{n-1}$ is the velocity of the particle at the $(n-1)$th collision, which obeys the relation derived from (25), that is,

$$\dot{u}_n=\dot{u}(\tau=\tau_n)=\frac{6\bar{A}}{k}+C_1^{(n-1)}\exp(-k\tau_n)+\frac{\bar{B}}{(1+k^2)^{1/2}}\sin(\tau_n+\theta)\ . \quad (29)$$

The velocity $\dot{u}_n$ at the nth collision can be determined by the preceding coupled recursion relations (27) and (29) when the initial conditions u_0 and $\dot{u}_0$ are given

The time τ_n at the nth collision obeys the recursion relation, which is derived from (27) and (29) by eliminating $\dot{u}_n$, that is,

$$\frac{1}{1-\exp(-k\tau_{n+1})}\left[6\bar{A}\left[\tau_{n+1}-\frac{1}{k}\right]+\left[\frac{6\bar{A}}{k}+\frac{k\bar{B}}{1+k^2}\right]\exp(-k\tau_{n+1})-\frac{k\bar{B}}{(1+k^2)^{1/2}}\cos(\tau_{n+1}+\theta)\right]$$
$$+\frac{\exp(-k\tau_n)}{1-\exp(-k\tau_n)}\left[6\bar{A}\left[\tau_n-\frac{1}{k}\right]+\left[\frac{6\bar{A}}{k}+\frac{k\bar{B}}{1+k^2}\right]\exp(-k\tau_n)-\frac{k\bar{B}}{(1+k^2)^{1/2}}\cos(\tau_n+\theta)\right]$$
$$=\frac{6\bar{A}}{k}-\left[\frac{6\bar{A}}{k}+\frac{k\bar{B}}{1+k^2}\right]\exp(-k\tau_n)+\frac{\bar{B}}{(1+k^2)^{1/2}}\sin(\tau_n+\theta)\ . \quad (30)$$

This is, however, the implicit relation between τ_n and τ_{n+1} and is not the simple mapping relation $\tau_{n+1}=F(\tau_n)$. Therefore we pay attention to the sequence of the velocity at successive collisions $\dot{u}_1,\dot{u}_2,\ldots,\dot{u}_n,\ldots$ described by (29) in the case of strong damping (k large) in order to obtain the map relation of $\dot{u}_n$'s.

The strong damping condition makes it possible to neglect the second terms on the left-hand side of Eq. (27). In addition, we further neglect the third term to eliminate the cosine dependence of τ_n for simplicity. This approximation leads to the simple relation

$$\tau_n\simeq-\frac{k}{6\bar{A}}C_2^{(n-1)}=\frac{\dot{u}_{n-1}}{6\bar{A}}+\frac{1}{k}\ . \quad (31)$$

This corresponds to the approximation in which τ_n can be represented by the linear function $\dot{u}_{n-1}$. If the velocity is large at the $(n-1)$th collision, the particle is reflected by the wall very strongly and kicked far away. Thus it takes a long time to collide again and τ_n becomes large. This simple relation leads to the mapping relation of $\dot{u}_n$'s from (29) as

$$\dot{u}_n=\frac{6\bar{A}}{k}-\left[\dot{u}_{n-1}+\frac{6\bar{A}}{k}+\frac{k\bar{B}}{1+k^2}\right]\exp\left[-\frac{k}{6\bar{A}}\dot{u}_{n-1}-1\right]+\frac{\bar{B}}{(1+k^2)^{1/2}}\sin\left[\frac{\dot{u}_{n-1}}{6\bar{A}}+\frac{1}{k}+\arctan k\right]\ . \quad (32)$$

The one-dimensional map $\dot{u}_n=F(\dot{u}_{n-1})$ of (32) is a smooth function of $\dot{u}$.

We have calculated the bifurcation diagram as a function of $\bar{B}$ in accordance with the map (32) for $k=1.0$ and $\bar{A}=1.2$. The variable $\dot{u}_n$ shows a period-doubling cascade to chaos as shown in Fig. 24, similar to the bifurcation sequence of the logistic map. In the chaotic region, $\dot{u}_n$'s reconstruct the mapping function (32) by plotting the successive point [Fig. 25(a)]. The motion of $\dot{u}_n$'s is bounded in a finite region. As shown in Fig. 25(b), the mapping function has a singular measure similar to the case of a Toda system.

Even the preceding simple model can yield chaos by the one-dimensional map. This is evidence that the asymmetry of the potential plays an important role in inducing chaos.[34] A particle coming back to the potential minimum at $u=0$ with modulation is kicked by the hard wall. The phases at the kicks are different at each collision to induce the intermittency of the motion of this particle.

In this section, we have shown the occurrence of chaos even in a simple one-dimensional map derived from the Toda system. This model is one dimensional and discrete so that it does not describe completely the dynamical behaviors of the original ordinary differential equation (ODE) system. However, it is valuable to discuss the role of the potential curvature so that chaos can be observed even in the limit of the asymmetric potential (23). This hard-wall model is an effective tool for investigating the

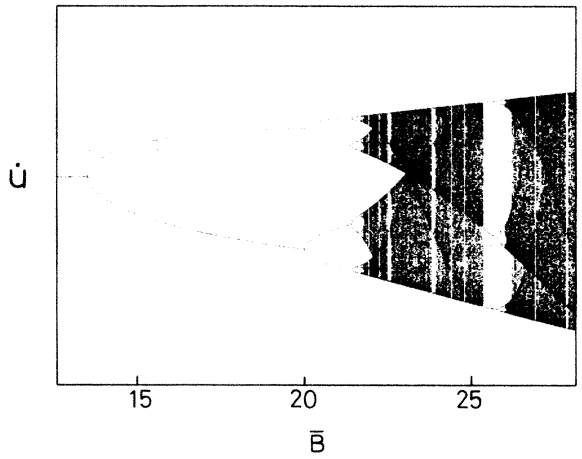

FIG. 24. Bifurcation diagram of the one-dimensional discrete dynamical system (32) for $k=1.0$ and $\bar{A}=1.2$. The period-doubling bifurcations and the periodic windows are observed as similar to the logistic (quadratic) map.

structure of the one-dimensional map contained in the differential equation (13) of the Toda particle. More precise and mathematical studies[35] on the bifurcation of the Toda system in terms of the chaotic dynamical system can be performed only by using this simple discrete model (32).

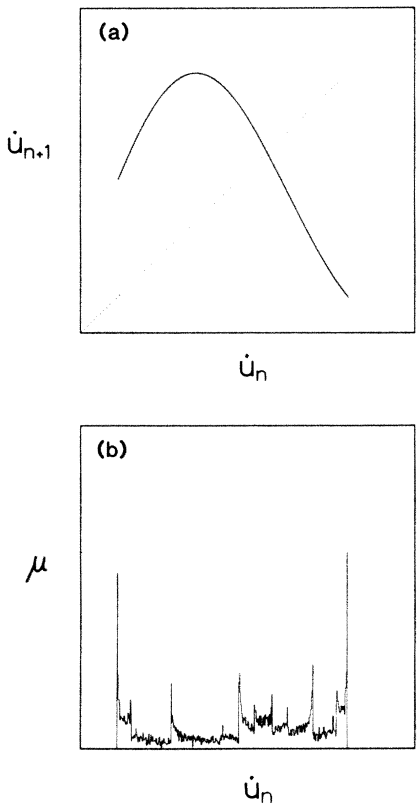

FIG. 25. (a) Return map constructed from the successive values of $\dot{u}_n$ for $k=1.0$, $\bar{A}=1.2$, and $\bar{B}=24.2$. (b) Invariant probability measure of the map (a).

V. CONCLUSIONS AND DISCUSSION

In this paper, we have presented the exact equivalence between the bad-cavity laser with modulated inversion and the damped and modulated Toda system. We can have a visible image by describing the spiking pulse train as the familiar sinusoidal wave in the Toda system. We have studied numerically the dynamical behaviors of the damped and modulated Toda system. The phase diagrams and the bifurcation diagrams have been obtained as a function of two control physical parameters: one is proportional to the modulation amplitude and the other is equivalent to the dc component of the population inversion. Numerical analysis makes it possible to choose arbitrary values of the control parameters and to investigate the characteristics of the chaotic responses. We can understand in detail the mechanisms of the onset of chaos in a laser under the strong modulation.

There are two kinds of onset of chaos: quasiperiodic mechanism and catastrophic crisis. The quasiperiodic instability comes after the incomplete or complete period-doubling bifurcations. Both the harmonic and the subharmonic oscillations are shown to exhibit quasiperiodic instability to chaos and crisis. Moreover, two kinds of chaos are observed: first is the quasiperiodic chaos in the vicinity of the quasiperiodic regions and second is the intermittent kicked chaos showing typical intermittent pulsations in a strong modulation case. The chaos in this Toda system is approximately described by the one-dimensional return map. Occurrence of chaos in a Toda system is understood also by the recursion relation derived analytically from the simple discrete model of this system. The one-dimensional map constructed from the hard-wall-potential model shows period-doubling cascade and chaos. Asymmetry of the potential curvature is found to play an important role in yielding a low-dimensional chaos.

Two key characteristics are examined in this paper: one is the quasiperiodic instability inducing chaos, another is the asymmetry of the potential function. The latter is shown to influence on yielding chaos by studying the discrete model of the Toda system. In terms of chaos, the dynamics under the strong modulation cannot be obtained by extrapolating the results of the analytic study[27] in the weak modulation case. Thus numerical study is an effective way to examine the strong nonlinear and nonautonomous system. Analytic and numerical investigations complement each other in the study of the nonlinear system as lasers.

Here we refer to the coexisting attractors. For example, the periodic windows within the regions of chaos are not always realized by the adiabatic sweeping of the control parameters. When several attractors coexist, their basins of attraction depend on the initial state. Therefore we must pay attention to the initial conditions in discussing the time evolution of the nonlinear system. It is so difficult to obtain the general analytic solutions of our model of the Toda system that the dynamical stability and realizability of each attractor coexisting in a phase space cannot be discussed analytically. In this paper the initial condition is fixed for each control parameter. Thus the coexistence or the competition between attrac-

tors and the structure of the basins of attraction cannot be clarified and are left for a future study.

Comparing these results of the numerical studies of the Toda system with those of the multimode laser in the bad cavity,[8,9] the role of the *phase* is found to be very important in discussing the dynamical properties of the laser emission. The phase dynamics are eliminated in this model by concerning ourselves with the exact resonant single mode. However, the phase should be given much attention as another degree of freedom in the nonresonant or the multimode cases. The resonant single-mode laser and the multimode laser are essentially different systems in terms of the dynamical properties of the phase. This is also shown as some differences between the phase diagram of these two systems. How chaos in a Toda system is modified by the phase motion is a future problem. In addition, the role of spontaneous emission in the temporal coherence of laser light is a controversial problem. The stochastic nature of spontaneous emission makes it impossible to treat the laser system as a deterministic dynamical system. Moreover, amplified spontaneous emission (ASE) and/or cooperative spontaneous emission (superradiance) are also important, especially in the experimental study of the bad-cavity laser. These are beyond the scope of our paper and are left for future studies.

The bad-cavity property can be realized experimentally by using the low-Q cavity. However, it is more difficult to operate the bad-cavity laser than the good-cavity one because of its high lasing threshold. Nevertheless, the bad-cavity conditions have been achieved by the far-infrared (FIR) laser (e.g., NH_3 laser, CH_2F_2 laser) or the molecular electronic transition laser (e.g., I_2 laser) in recent experiments.[36–38] Here we must pay attention to the *spatial* coherence of the laser emission. In this paper we assume *a priori* the plane-wave profile of the transverse structure of the laser-light beam. However, the bad-cavity property (low Q value) may reduce the spatial coherency and make the plane-wave approximation invalid. The spatial characteristics of the laser light become important not only in the experiments but also in terms of spatiotemporal chaos.[39] This is also to be clarified in the future.

It is interesting to test experimentally the results of our investigations. Candidates to observe quasiperiodic instability and two kinds of chaotic emission (quasiperiodic and intermittent kicked) are the lasers previously mentioned. We must control the ratio $\gamma_{\parallel}/\omega_m$ arbitrarily in addition to the dc component of the population inversion and the modulation amplitude. We hope that the two kinds of chaos have a good potential for widespread application also from an engineering point of view; for example, information processing[40] or the temporal incoherent light source for laser spectroscopy.[4–6] These applications can be expected only when continuous control of the cavity quality and the relaxation rates of the materials is achieved.

ACKNOWLEDGMENTS

The author would like to thank Dr. K. Otsuka and Dr. N. Nagaosa for fruitful discussions. He also acknowledges Professor E. Hanamura and Professor J. Satsuma for discussions, critical readings of this manuscript, and continual encouragement. Numerical computations have been carried out by HITAC M-682H and S-810 of the Computer Center of the University of Tokyo. This work has been supported in part by Scientific Research Grant-in-Aid No. 61214003 for special project research on "alloy semiconductor physics and electronics," from the Ministry of Education, Science and Culture of Japan.

[1]The special issue on the *Instabilities in Active Optical Media,* J. Opt. Soc. Am. B **2**, No. 1 (1985).

[2]*Optical Instabilities,* edited by R. W. Boyd, M. G. Raymer, and L. M. Narducci (Cambridge University Press, London, 1986).

[3]*Instabilities and Chaos in Quantum Optics,* Vol. 34 of *Springer Series in Synergetics,* edited by F. T. Arecchi and R. G. Harrison (Springer-Verlag, Berlin, 1987).

[4]N. Morita and T. Yajima, Phys. Rev. A **30**, 2525 (1984); N. Morita, T. Tokizaki, and T. Yajima, J. Opt. Soc. Am. B **4**, 1269 (1987).

[5]S. Asaka, H. Nakatsuka, F. Fujiwara, and M. Matsuoka, Phys. Rev. A **29**, 2286 (1984).

[6]R. Beach, D. DeBeer, and S. R. Hartmann, Phys. Rev. A **32**, 3467 (1985).

[7]T. Ogawa and E. Hanamura, Opt. Commun. **61**, 49 (1987).

[8]T. Ogawa and E. Hanamura, Appl. Phys. B **43**, 139 (1987).

[9]T. Ogawa and E. Hanamura (unpublished).

[10]E. N. Lorenz, J. Atmos. Sci. **20**, 141 (1963).

[11]H. Haken, Phys. Lett. **53A**, 77 (1975).

[12]In the case of the good cavity, dynamical properties of the modulated lasers have been partially clarified as shown in Refs. 13–19.

[13]W. Klische, H. R. Telle, and C. O. Weiss, Opt. Lett. **9**, 561 (1984).

[14]H. J. Scholz, T. Yamada, H. Brand, and R. Graham, Phys. Lett. **82A**, 321 (1981).

[15]J. R. Tredicce, F. T. Arecchi, G. P. Puccioni, A. Poggi, and W. Gadomski, Phys. Rev. A **34**, 2073 (1986).

[16]Chang-Hee Lee, Tae-Hoon Yoon, and Sang-Yung Shin, Appl. Phys. Lett. **46**, 95 (1985).

[17]M. Tang and S. Wang, Appl. Phys. Lett. **48**, 900 (1986).

[18]T. Erneux, S. M. Baer, and P. Mandel, Phys. Rev. A **35**, 1165 (1987).

[19]P. Mandel, P. Nardone, and T. Erneux (unpublished).

[20]M. Toda, J. Phys. Soc. Jpn. **22**, 431 (1967); **23**, 501 (1967).

[21]See, for example, C. Hayashi, *Nonlinear Oscillations in Physical Systems* (McGraw-Hill, New York, 1964).

[22]N. N. Bogoliubov and Y. A. Mitropolsky, *Asymptotic Methods in the Theory of Non-linear Oscillations* (Gordon and Breach, New York, 1961).

[23]I. I. Satija, A. R. Bishop, and K. Fesser, Phys. Lett. **112A**, 183 (1985).

[24]T. Klinker, W. Mayer-Ilse, and W. Lauterborn, Phys. Lett. **101A**, 371 (1984).

[25]J.-P. Eckmann and D. Ruelle, Rev. Mod. Phys. **57**, 617 (1985).
[26]J. M. T. Thompson and H. B. Stewart, *Nonlinear Dynamics and Chaos* (Wiley, New York, 1986).
[27]T. Ogawa (unpublished).
[28]This point is different from the case of the multimode laser in Refs. 7–9.
[29]The connection between the Toda potential and the laser system under the rate-equation approximation has been reported in Refs. 30 and 31.
[30]G. L. Oppo and A. Politi, Z. Phys. B **59**, 111 (1985).
[31]A. M. Ratner, *Spectral, Spatial, and Temporal Properties of Lasers* (Plenum, New York, 1972).
[32]C. Grebogi, E. Ott and J. A. Yorke, Physica (Utrecht) **7D**, 181 (1983).
[33]See also Y. H. Kao, J. C. Huang, and Y. S. Gou, Phys. Rev. A **35**, 5228 (1987).
[34]J. W. Swift and K. Wiesenfeld, Phys. Rev. Lett. **52**, 705 (1984).
[35]V. K. Melnikov, Trans. Moscow Math. Soc. **12**, 1 (1963).
[36]C. O. Weiss, J. Opt. Soc. Am. B **2**, 137 (1985).
[37]C. O. Weiss and J. Brock, Phys. Rev. Lett. **57**, 2804 (1986).
[38]T. Q. Wu and C. O. Weiss, Opt. Commun. **61**, 337 (1987).
[39]See the special issue on the Spatio-temporal Coherence and Chaos in Physical Systems, Physica (Utrecht) **23D** (1986).
[40]J. S. Nicolis, Rep. Prog. Phys. **49**, 1109 (1986).

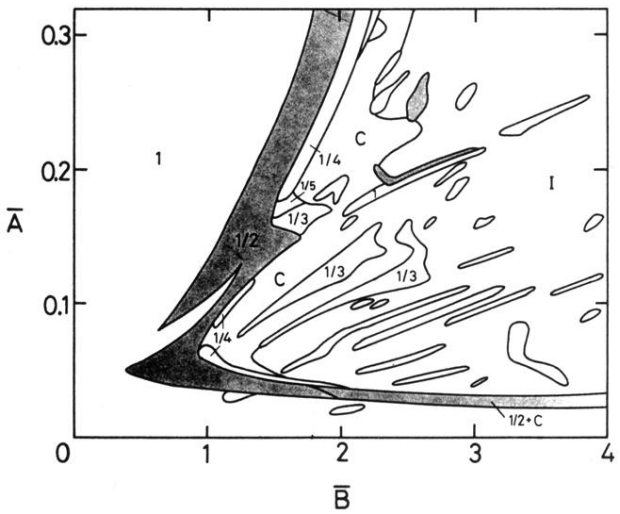

FIG. 18. Phase diagram of modulation characteristics under the condition $k=0.1$ in the two-dimensional parameter space $\overline{A}$ and $\overline{B}$, corresponding to $A\in[1,5.8]$ and $B\in[0,10]$. The subharmonic oscillation of order $\frac{1}{2}$ is observed in the dark regions. The islandlike structure is due to the several periodic windows. This phase diagram is also coarse grained.

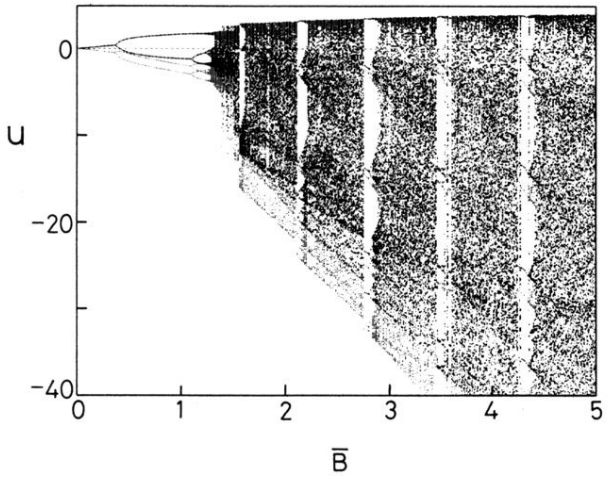

FIG. 19. Bifurcation diagram of u against the modulation amplitude $\bar{B}$ for $k=0.1$ and $\bar{A}=0.05$.

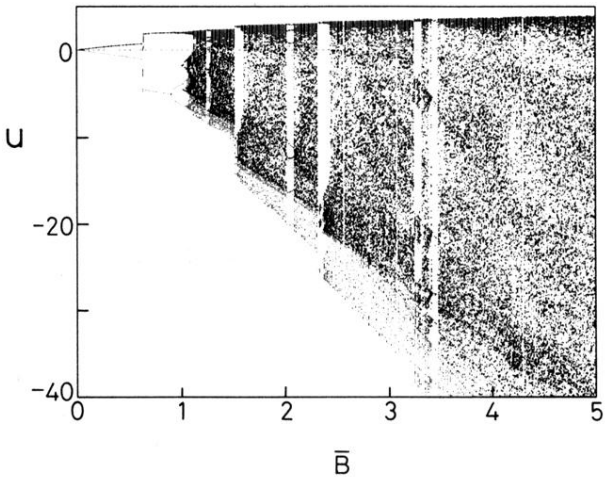

FIG. 20. Bifurcation diagram of u for $k=0.1$ and $\bar{A}=0.08$.

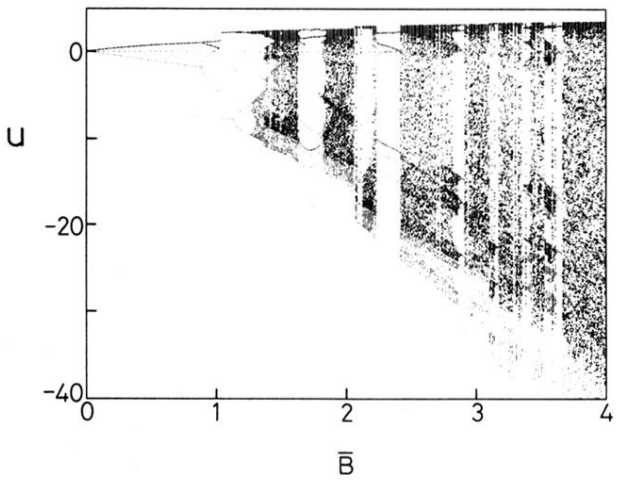

FIG. 21. Bifurcation diagram of u for $k=0.1$ and $\overline{A}=0.11$.

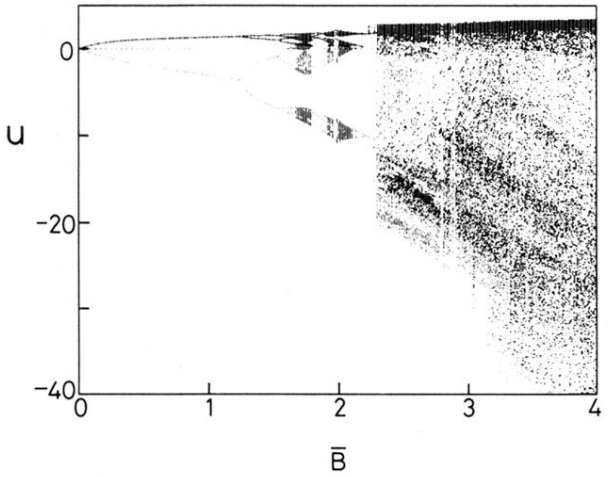

FIG. 22. Bifurcation diagram of u for $k=0.1$ and $\overline{A}=0.18$.

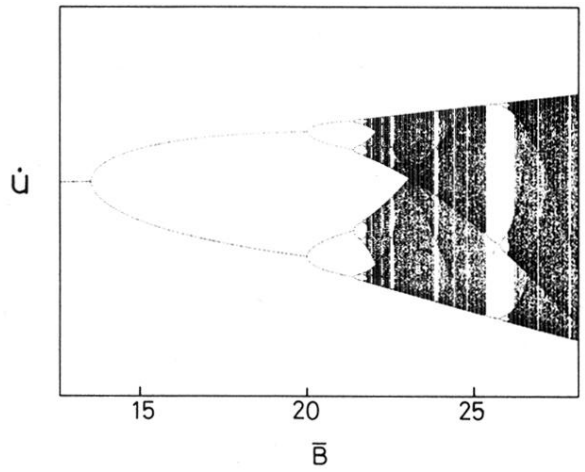

FIG. 24. Bifurcation diagram of the one-dimensional discrete dynamical system (32) for $k = 1.0$ and $\overline{A} = 1.2$. The period-doubling bifurcations and the periodic windows are observed as similar to the logistic (quadratic) map.

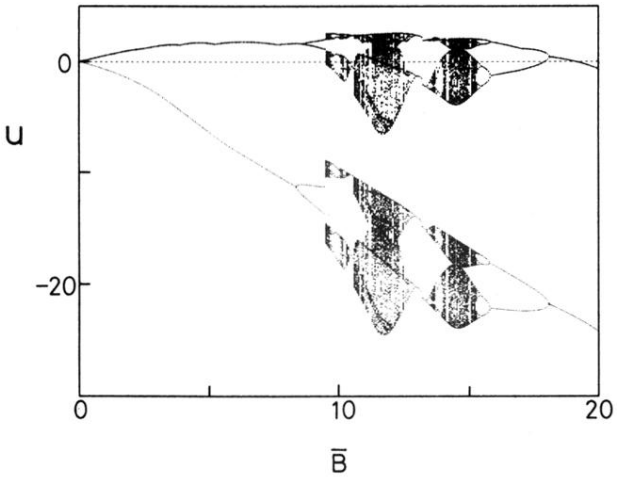

FIG. 4. Bifurcation diagram of u for $k=1.0$ and $\overline{A}=0.4$.

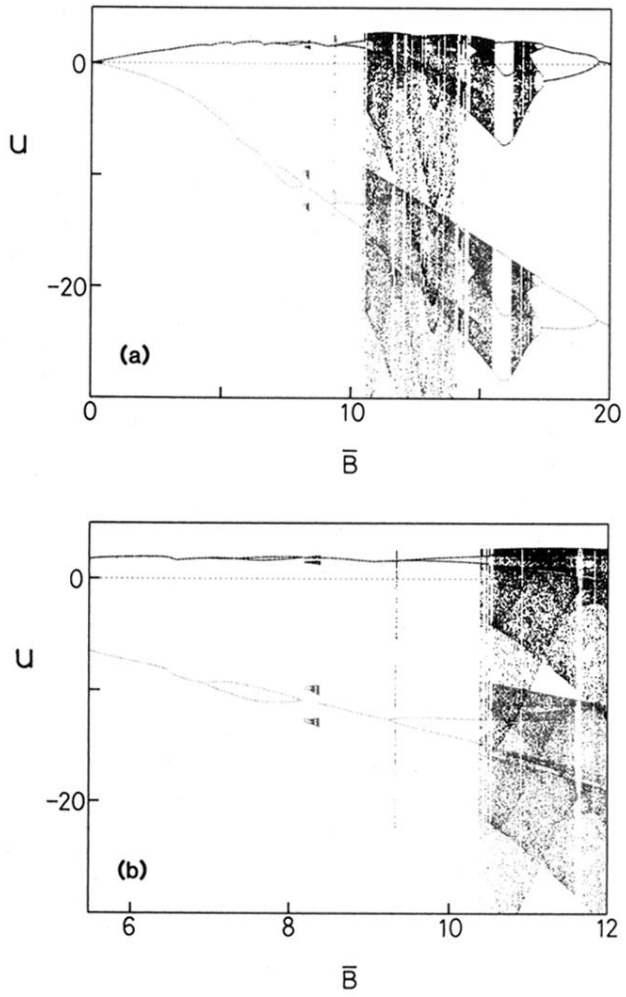

FIG. 5. (a) Bifurcation diagram of u for $k=1.0$ and $\overline{A}=0.5$. (b) Enlargement of the region of the onset of chaos. The catastrophic change to chaos is observed at $\overline{B}=10.5$.

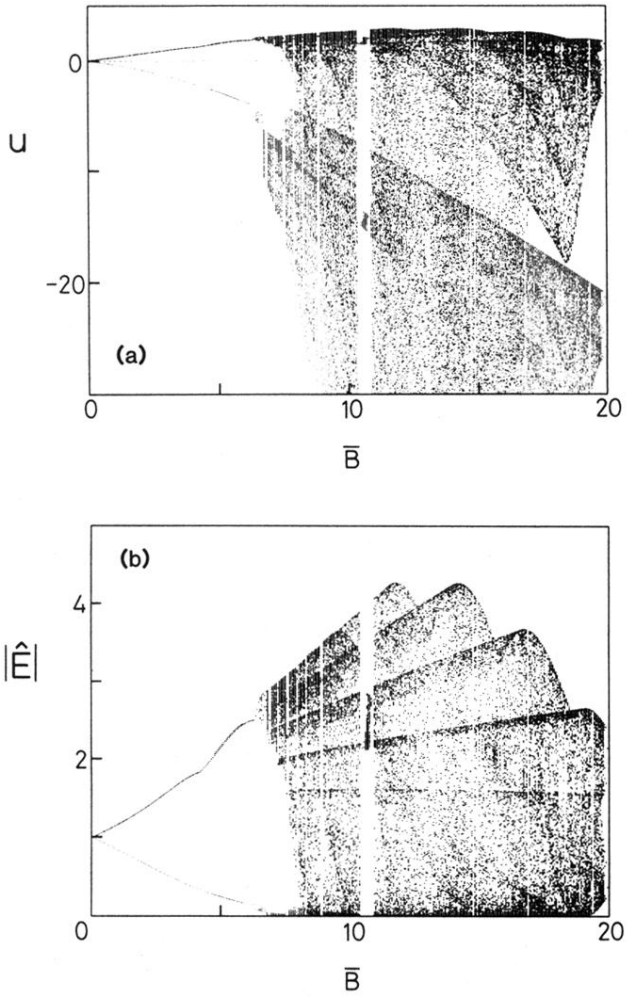

FIG. 6. (a) Bifurcation diagram of u for $k=1.0$ and $\overline{A}=0.7$. The harmonic oscillation yields the quasiperiodic instability at $\overline{B}=6.5$. (b) The corresponding bifurcation diagram of the amplitude of the field $|\hat{E}|$.

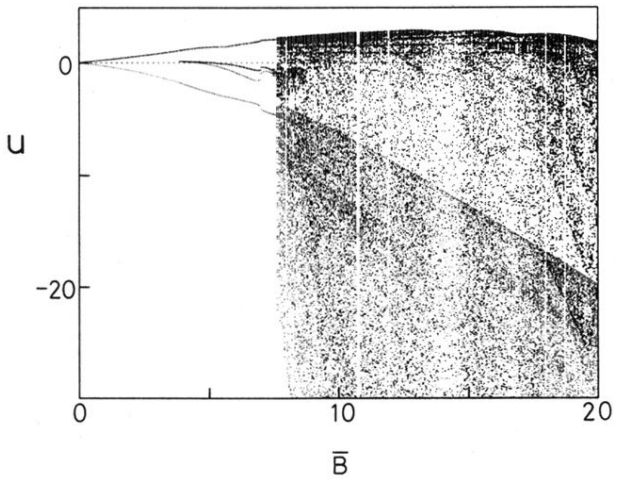

FIG. 7. Bifurcation diagram of u for $k=1.0$ and $\overline{A}=0.8$.

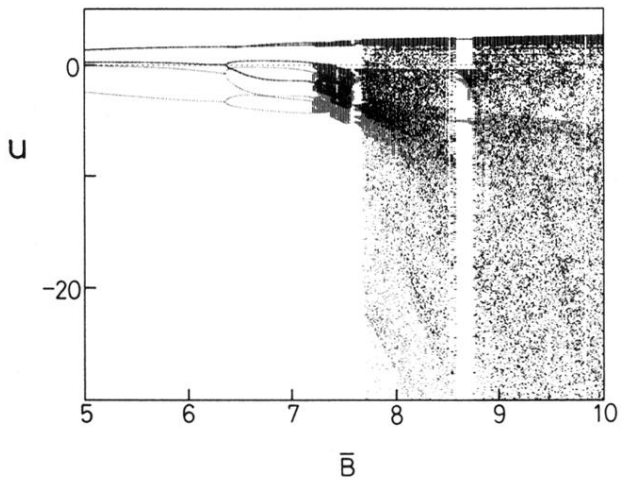

FIG. 8. Bifurcation diagram of u for $k=1.0$ and $\overline{A}=0.9$.

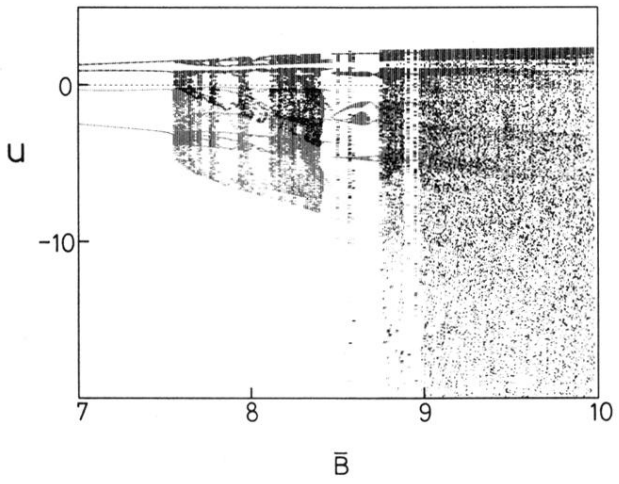

FIG. 9. Enlargement of the bifurcation diagram of u for $k = 1.0$ and $\overline{A} = 1.3$.